Effect of confinement on the rotation of a two-dimensional elliptical porous particle in shear flow

Cite as: Phys. Fluids **33**, 083317 (2021); doi: 10.1063/5.0054660 Submitted: 20 April 2021 · Accepted: 24 July 2021 · Published Online: 12 August 2021







Jiajia Liu (刘佳佳),^{1,2} <mark>向</mark> Chenggong Li (李承功),¹ Yunxin Zhang (张鋆鑫),^{1,2} Mao Ye (叶茂),^{1,a)} <mark>向</mark> and Zhongmin Liu (刘中民)¹

AFFILIATIONS

- ¹Dalian National Laboratory for Clean Energy, National Engineering Laboratory for MTO, Dalian Institute of Chemical Physics, Chinese Academy of Sciences, Dalian 116023, China
- ²University of Chinese Academy of Sciences, Beijing 100049, China

ABSTRACT

The rotation of non-spherical porous particles in fluid flows is of practical relevance in various natural and industrial processes. However, despite the increasing interest in micro-scale channels and reactors, the understanding of rotation of non-spherical porous particles in a confined fluid flow is, if not blank, far from complete. In this work, we present a numerical study on the rotation of an elliptical porous particle in a confined shear flow by solving the governing equations using a lattice Boltzmann method. The particles with varying aspect ratios AR, Darcy number Da, and Reynolds number Re are examined for different confinement ratios B. Akin to its solid counterpart, the elliptical porous particle either exhibits time-periodic rotation with a non-uniform angular rate or takes a stationary orientation for different B. With finite fluid inertia, both the maximum and minimum angular rate decrease with B. For the elliptical porous particle, a higher B promotes the increasing rate of rotation period against Re, resulting in a smaller critical Reynolds number Re_c (if observed) at which the particle ceases to rotate. A scaling law for solid particles was extended to correlate the rotation period and Re for porous particles, where B has a negligible effect. An empirical formula to predict Re_c as a function of B, AR, and Da is established using the symbolic regression. The transition from rotating to stationary at different B can be explained by the net torque exerted on the elliptical porous particle.

Published under an exclusive license by AIP Publishing. https://doi.org/10.1063/5.0054660

I. INTRODUCTION

The solid–fluid flows of non-spherical particles are of practical relevance in a variety of natural and industrial processes, such as ice crystals in the cloud formation, planktons in the ocean, microplastics in the marine environment, flocs in waste water treatment, catalyst clusters in fluidized bed reactors, and paper-making processes. In particular, the rotational behaviors of these non-spherical particles are crucial to understanding and controlling these applications, which, however, have received little attention because the effective experimental and modeling methods are still lacking. Early studies on the rotation of particles were mainly based on the analytical methods. In the regime of Stokes flow, Jeffery first investigated analytically the motion of a single solid ellipsoid suspended in an unbounded simple shear flow via a quasi-steady approach, where the fluid inertia was completely neglected. He also derived analytical equations for the inertia-free spheroid and showed that the spheroid in the simple

shear flow rotates periodically with a non-uniform rotation rate. Following Jeffery's pioneering work, many research studies regarding the dynamic behaviors of particles with different particle shapes such as circular cylinders, ellipsoids, dumb-bell shaped particles, and rod-like particles were further conducted using various analytical methods such as inner and outer asymptotic expansion, perturbation theory, and reciprocal theorem. These early theoretical works, however, are limited to the rotation of particles at sufficiently low Reynolds numbers. In real applications, the effects of the fluid inertia cannot be ignored. In particular, owing to the rapid development of micro-reactors and among many others in the past decades, the understanding of the rotation of non-spherical particles in fluid flow that is essentially confined, despite the significance, is far from complete.

In recent years, numerical simulations have grown to be an important scientific tool to complement traditional experimental

a) Author to whom correspondence should be addressed: maoye@dicp.ac.cn

approaches, such as the finite-difference method, 12 lattice Boltzmann method (LBM), 13,14 and fictitious domain method. 15 Both experimental and numerical approaches can overcome the shortcoming of analytical methods and describe systems with finite fluid inertia and confinement. For moderate Reynolds numbers, Kossack and Acrivos 12 presented numerical data for the two-dimensional simple shear flow past a circular cylinder by solving the Navier-Stokes equations with a finite-difference method for the shear Reynolds number up to 70. Results show that the dimensionless rotation rate of the torque-free circular cylinder decreases with Re as $Re^{-1/2}$, where the influence of confinement is negligible because a free boundary condition corresponding to infinite confinement is assumed. Later on, Poe and Acrivos¹⁶ studied experimentally a cylinder and a sphere freely rotating in a simple shear flow with three different confinement ratios H/r = 6.32, 10.8, and 11.24 for Re up to 21.1, where H is the channel height and r is radius of the particle, respectively. Their results reveal that the confinement of the walls affects the rotation rate of particles, which, however, is not discussed in detail. For Re up to about 10, the rotating data for the cylinder is found to be in agreement with the numerical results obtained by Kossack and Acrivos. 12 Also, Ding and Aidun¹³ investigated numerically the effect of inertia on the dynamics of a single circular cylinder and elliptical cylinder, as well as a single ellipsoid immersed in simple shear flows by the lattice Boltzmann method (LBM). For a circular cylinder, they demonstrated that the dimensionless rotation rate increases with the height of the channel for a low Reynolds number, and the decreasing rate of the dimensionless rotation rate with Re becomes larger with the increase in the height of the channel for higher Re. In addition, for both the elliptical cylinder and the ellipsoid, they observed a transition from a rotation state to a stationary orientation at a critical Reynolds number (Re_c) and further proposed a scaling law to correlate the dimensionless rotation period and Re for a fixed confinement ratio. Following Ding and Aidun's work, Zettner and Yoda¹⁷ first investigated experimentally a neutrally buoyant circular cylinder freely rotating in a simple shear flow using particle-image velocimetry (PIV). They presented their results at the particle shear Reynolds number ranging from 8 to 25 at two different confinement ratio values. Their results showed that the rotation rate decays with Re, with the rate of decay increasing as the confinement effect weakens, which is consistent with the numerical results reported by Ding and Aidun.¹³ Moreover, they further investigated experimentally with PIV the effects of fluid inertia, flow confinement, and aspect ratio (AR) of particles on the dynamics of a neutrally buoyant elliptical cylinder suspended in a simple shear flow for moderate Re. 18 Their experimental results confirmed the LBM simulations for an elliptical cylinder with an aspect ratio of 2 by Ding and Aidun. 12 Besides, they showed that Re_{cr} decreases as the confinement effect weakens and the aspect ratio increases.

Later, Qi and Luo¹⁹ reported the results of simulations using LBM on the rotation of a neutrally buoyant prolate or oblate spheroid suspended in a Couette flow and found several distinctive rotation states depending on *Re* and particle shape. Lundell and Carlsson²⁰ investigated a heavy ellipsoid in creeping shear flow, focusing on the transition of the particle rotation rate and orbit shape. They demonstrated that the particle motion is affected strongly by the Stokes number and initial orientations. Lundell²¹ and Rosen *et al.*²² reported, respectively, the effects of particle inertia and fluid inertia on the dynamics of triaxial ellipsoids in simple shear flows. Rosen *et al.*²³

conducted quantitative analysis on the angular dynamics of a spheroid in shear flow with fluid inertia and showed that the analysis can provide an accurate description of stable rotational states. Recently, Cui et al. 24 investigated theoretically the rotational dynamics of ellipsoids in simple shear flow by the Floquet analysis and found some stable states for both axis-symmetric spheroids and tri-axial ellipsoids. Additionally, Huang et al. 15 investigated numerically with a fictitious domain method a neutrally buoyant elliptical particle freely rotating in a simple shear flow and focused on the effects of confinement of bounding walls for particles with different aspect ratios. They demonstrated that the increase in either the aspect ratio or confinement ratio could lead to the decrease in Re_{cr} where the dynamic mechanism is distinct.

All the above research studies exclusively focused on solid particles, including circular cylinders, elliptical particles, and ellipsoids. In practice, however, particles with porous structures are widely encountered in industrial processes. The complex porous structure of permeable particles strongly affects the interactions between particles and fluid because the fluid penetrates through the porous media and thus complicates the structures of the particle-fluid system. Therefore, understanding of dynamic behaviors of porous and permeable particles in simple shear flows is critically important for various industrial processes.

For the rotation of porous particles, Masoud et al. 25 studied theoretically a porous ellipsoid freely rotating in a simple shear flow at vanishing Re based on the Brinkman equation. Their results demonstrated that the permeability has a negligible effect on the rotational behaviors of porous particles. However, as the two popular models used for simulating porous particles, both Darcy's law and the Brinkman equation are limited to cases where the *Re* of the fluid flows is sufficiently low, such as creeping flow, because the nonlinear inertial term is neglected in these two models. The inertia effect plays an important role in the motion of porous particles in various practical applications. Recently, Wang et al.²⁶ proposed a new momentum equation named volume-averaged macroscopic equation in terms of the intrinsic phase averaged velocity, where the time derivative and the nonlinear inertial term are included. Therefore, the volume-averaged macroscopic equation can be used to describe fluid flows through the moving porous media at finite Re. The volume-averaged macroscopic equation has been used in some works. 14,27-29 Recently, Li et al. 27 investigated the rotational behaviors of a circular porous particle suspended in a simple shear flow for Re up to 108 based on the volumeaveraged macroscopic equation, which is numerically solved by LBM. They confirmed the conclusion of Masoud et al.25 that the permeability has little effect on the rotational behavior of porous particles at vanishing Re when the effects of confinement can be neglected. And they further revealed that the effects of permeability cannot be neglected when the fluid inertia or the confinement effect is not negligible for circular porous particles. Following the work of Li et al., we further studied the rotation of an elliptical porous particle in a simple shear flow, focusing on the effects of permeability and fluid inertia.

In practical experiments, the fluid flow is always confined by boundary walls. Meanwhile, the numerical simulations are mostly conducted within relatively small domains due to the limitation of computational power. Therefore, confinement is an important issue in these particulate two-phase flows. Understanding the confinement effects on the rotational dynamics of elliptical porous particles in a

simple shear flow can provide significant insights into the fluid flows with suspended porous particles and contribute a first yet fundamental step for many complex phenomena. Previous results have shown that the confinement plays a crucial role in determining the rotational dynamics of solid particles ^{13,15,18} and circular porous particles in simple shear flows. ²⁷ Compared with solid or circular porous particles, the confinement effects on the rotational dynamics might be more complicated for non-spherical porous particles, which therefore motivates our work reported in this paper. The objective of this work is to investigate the effects of confinement on the rotational behaviors of neutrally buoyant elliptical porous particles in a simple shear flow. In this work, we adopt the volume-averaged macroscopic equation ²⁶ to formulate fluid flows inside and outside the porous media, which is numerically solved by the LBM.

II. GOVERNING EQUATIONS

In this study, we consider a neutrally buoyant elliptical porous particle suspended in a two-dimensional simple shear flow. The schematic diagram of the elliptical porous particle freely rotating in a simple shear flow is shown in Fig. 1. The computational domain is a rectangular channel with width W and height H. The aspect ratio (AR) of the elliptical particle is defined as AR = a/b, where a and b are the semi-major and semi-minor axes of the particle, respectively. The shear flow is driven by two bounding walls, which are located along the width direction and moving in the opposite directions with the same velocity U. Here, Re is the particle shear Reynolds number given by $Re = \Gamma D^2/\nu$, where Γ is the shear rate with $\Gamma = 2U/H$, ν is the kinematic viscosity of the fluid, and D is set as D = 2a following Ref. 14. The confinement ratio (B) is defined as B = H/D. In this work, the particle shear Reynolds number Re rather than the channel Reynolds number $Re_{ch} = UH/2v$ is chosen to account for the effects of fluid inertia. The reasons are twofold. On the one hand, Re is more appropriate to characterize the fluid inertia for a simple shear flow past a freely rotating particle, following literatures. 13,15,18,27-29 On the other hand, the channel Reynolds number Rech is a function of Re and the confinement ratio B, and the direct use of Re and B can, respectively, reflect the effects of the fluid inertia and confinement in a straightforward manner.

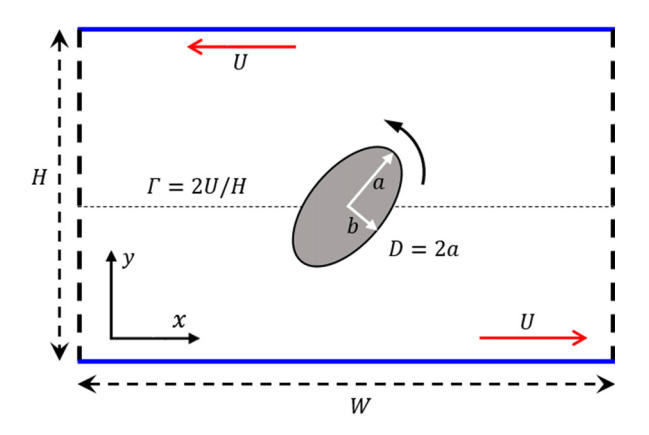


FIG. 1. The schematic diagram of the elliptical porous particle freely rotating in a simple shear flow.

The neutrally buoyant elliptical porous particle is assumed to be homogeneous and isotropic in the porous structure and immersed in an incompressible Newtonian fluid. We employ the volume-averaged macroscopic equations²⁶ in terms of the intrinsic phase average velocity to describe fluid flows inside and outside the porous particle. The macroscopic governing equations are derived by averaging the microscopic continuity and momentum equations inside the porous particle over a representative elementary volume (REV). It is noteworthy that the size of the REV is much larger than the pore size and much smaller than the particle domain. The macroscopic governing equations where the transient term and the nonlinear inertial term are taken into account can be written as

$$\nabla \cdot \langle \mathbf{u}_f \rangle^f = 0, \tag{1}$$

$$\rho_f \left[\frac{\partial \langle \mathbf{u}_f \rangle^f}{\partial t} + \langle \mathbf{u}_f \rangle^f \cdot \nabla \langle \mathbf{u}_f \rangle^f \right] = -\nabla \langle p_f \rangle^f + \mu \nabla^2 \langle \mathbf{u}_f \rangle^f + \mathbf{F}_m, \quad (2)$$

where ρ_f is the fluid density, μ is the fluid dynamic viscosity, and $\langle u_f \rangle^f$ and $\langle p_f \rangle^f$ are the intrinsic phase averaged velocity and pressure of fluid phase, respectively. The intrinsic phase average is defined by

$$\langle \psi_k \rangle^k = \frac{1}{V_k} \int_{V_k} \psi_k dV, \tag{3}$$

where V_k is the volume of the k-phase inside the representative volume V and ψ_k is a quantity related to the k-phase (k refers to either f or s denoting the fluid phase or particle phase, respectively). With the translational velocity U_p and rotational velocity w_p , the skeleton of the isotropic and homogeneous elliptical porous particle moves rigidly with velocity $u_s = U_p + w_p \times (r - R)$, where r is the position vector within the particle, and R is the position vector of the mass center of the particle. Since the porous particle moves with a rigid-body motion, the translational velocity U_p and rotational velocity w_p remain unchanged after taking the intrinsic phase average. Therefore, the intrinsic phase averaged velocity of particle phase $\langle u_s \rangle^s = u_s = U_p + w_p \times (r - R)$ can be obtained. For simplicity, $\langle u_s \rangle^s$ is denoted by V_p in the following. F_m is the total body force which can be calculated via

$$\mathbf{F}_{m} = -\frac{\varepsilon\mu}{K} \left(\langle \mathbf{u}_{f} \rangle^{f} - \mathbf{V}_{p} \right) - \rho_{f} \frac{\varepsilon^{2} F_{\varepsilon}}{\sqrt{K}} \left(\langle \mathbf{u}_{f} \rangle^{f} - \mathbf{V}_{p} \right) \left| \langle \mathbf{u}_{f} \rangle^{f} - \mathbf{V}_{p} \right| + \rho_{f} \mathbf{G},$$
(4)

where G is the gravitational force and ε and K are the porosity and permeability of the particle, respectively. Note that the permeability and porosity are two parameters to describe the porous structure inside the elliptical porous particle. In this work, K is associated with ε via $K = \varepsilon^3 d_p^2/[150(1-\varepsilon)^2]$, where d_p represents the characteristic diameter of filling grains within the elliptical porous medium, which is taken as 100 μ m following Bhattacharyya *et al.*³¹ In the limiting case of $\varepsilon = 0$, i.e., the porous particle reduces to a solid particle, the permeability K which quantifies the ability of porous particle to transmit fluid approaches to 0. Whereas as $\varepsilon = 1$, which means that the porous particle is fully filled with fluid, the value of K becomes infinite. The governing equations (volume-averaged macroscopic equations) used in this work can describe the fluid flows in the whole flow field, including the region occupied by the porous particle, through adjusting the value of porosity ε . The porosity takes $\varepsilon = 1$ for the pure fluid region

outside the elliptical porous particle and $\varepsilon=0\sim 1$ for the region inside. The porous structure of the particle is depicted by Da, which is defined as

$$Da = K/L_{ref}^2, (5)$$

where L_{ref} is the characteristic length of particle and is taken as $2\sqrt{ab}$ for the elliptical particle. F_{ϵ} denotes the geometric function, which follows Ergun's correlation³² $F_{\epsilon} = 1.75/\sqrt{150\epsilon^3}$. The Newton's equations used to describe the translational and rotational motions of the particle are given by

$$F_p = M_p \frac{dU_p}{dt}, \tag{6}$$

$$T_p = I_p \frac{d\mathbf{w}_p}{dt},\tag{7}$$

where U_p is the translational velocity, w_p is the rotational velocity, M_p is the particle mass, I_p is the moment of inertia of particles, and F_p and T_p are the net force and torque acting on the porous particle, respectively. LBM which is employed to solve the macroscopic governing equations (1) and (2) is presented in Appendix A.

III. MODEL VALIDATION

To validate our model, we compare our simulation results for a neutrally buoyant elliptical particle fixed or freely rotating in a simple shear flow with analytical solutions or results previously reported in the literature. Here, three validation cases are considered: fixed elliptical porous particles with different aspect ratios in a simple shear flow and freely rotating elliptical particles in a simple shear flow at small and finite Re. The semi-minor axis of the elliptical porous particle is set to $b=0.04\,\mathrm{cm}$, and the semi-major axis a=AR*b. The elliptical porous particle is initially placed in the geometric center of the rectangular channel with height H=20a and width W=2H, which ensures that the channel boundaries do not affect simulations. 360 lattices are used to resolve 1 cm after checking the grid independence. Table I shows the simulation parameters used in the model validation, with NX and NY being the grid dimension in x and y axis, respectively.

First, the torque T_q exerted on the fixed elliptical porous particles with different aspect ratios AR of 2, 2.5, and 3 by the simple shear flow at Re=0.08 is investigated. The results by Masoud $et\ al.^{25}$ show that the aspect ratio of elliptical porous particles has negligible effects on the torque without fluid inertia and they further gave the analytical solution as

$$T_q = 2\pi\mu\Gamma a^2 \frac{I_2(\beta)}{I_0(\beta)},\tag{8}$$

TABLE I. Parameters used in simulations of model validation.

Re	τ	b/cm	a/cm	AR	H/cm	W/cm	NX	NY
0.08	0.8	0.04	0.08 0.10 0.12	2.5	1.6 2.0 2.4	3.2 4.0 4.8	720	1152 1440 1728

where $\beta=\sqrt{ab/K}=0.5\sqrt{1/Da}$, and both I_0 and I_2 are modified Bessel functions of the first kind. For the sake of consistency, the dimensionless torque $T_q/2\pi\mu\Gamma a^2$ is plotted as a function of Da in Fig. 2. As can be seen, the curves of $T_q/2\pi\mu\Gamma a^2$ vs Da practically overlap for elliptical porous particles with AR=2, 2.5, and 3, and they all agree well with the analytical solutions shown by the solid line, indicating that the implementation of permeability of our numerical model is accurate.

Next, the angular rate of an elliptical particle in a simple shear flow at vanishing Re is examined. Here, Da is fixed at $Da = 10^{-10}$, i.e., the elliptical porous particle can be treated as its solid impermeable counterpart. Re is set to 0.08; therefore, the fluid inertia can be neglected. In this way, a comparison can be made with analytical solutions for a solid impermeable elliptical particle. Jeffery derived the analytical solution for the rotation of a solid 3D spheroid in a simple shear flow. Actually, it was found that Jeffery's solution is independent of one principal axis of the ellipsoid around which the ellipsoid rotates, and this axis is parallel to the vorticity vector of the plane of the 2D simple shear flow. If this principal axis of the ellipsoid is extended to infinity, the ellipsoid can be reduced to an elliptical cylinder. In this sense, Jeffery's solution also applies to 2D elliptical particle, which was confirmed by Feng and Joseph³³ and Ding and Aidun.¹³ Following Jeffery, the analytical solution of angular rate $\dot{\chi}$ of 2D solid elliptical particles with various aspect ratios suspended in shear flow without fluid inertia can be written as

$$\dot{\chi} = \frac{\Gamma}{a^2 + b^2} \left(a^2 \cos^2 \chi + b^2 \sin^2 \chi \right). \tag{9}$$

The comparisons of dimensionless angular rate $\dot{\chi}/\Gamma$ of the elliptical particles with aspect ratios AR of 2, 2.5, and 3 obtained by our simulations with analytical solutions⁷ are presented in Fig. 3. It is shown that the elliptical particles with different aspect ratios exhibit time-periodic rotational behavior with non-uniform angular rates, which are in good agreement with Jeffery's solution.⁷

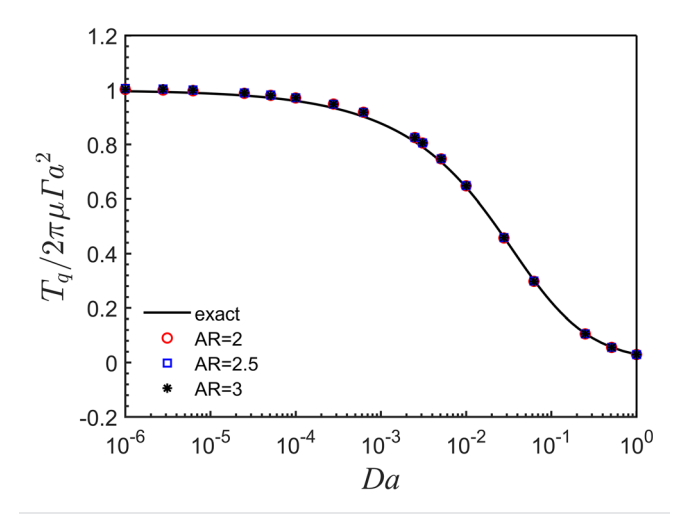


FIG. 2. Dimensionless torque $T_q/2\pi\mu\Gamma a^2$ exerted on the fixed elliptical porous particle with different aspect ratios of 2, 2.5, and 3 as a function of *Da* where Re=0.08.

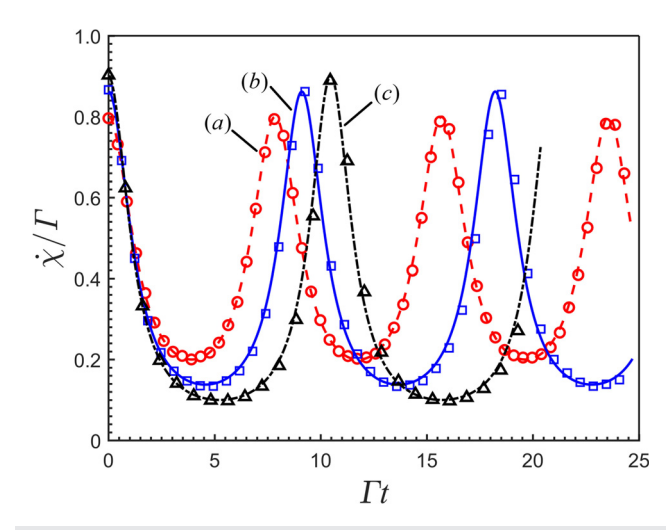


FIG. 3. Dimensionless angular rate $\dot{\chi}/\Gamma$ of the elliptical particle freely rotating in the simple shear flow at Re=0.08 and $Da=10^{-10}$ as a function of dimensionless time Γt : (a) AR=2, (b) AR=2.5, and (c) AR=3. The lines are analytical solutions developed by Jeffery, and scatters denote our simulation results.

Moreover, the angular rate and the corresponding rotation period of the elliptical particle with an aspect ratio of 2 suspended in a simple shear flow at *Re* up to 30 are checked. We find that our simulations are highly consistent with the results reported by Ding and Aidun. ¹³ For conciseness, details are not presented here, and readers can refer to our previous work³⁰ for further information.

IV. RESULTS AND DISCUSSION

The rotations of a neutrally buoyant elliptical solid and porous particle initially placed at the geometric center of the unbounded shear flow where the confinement ratio B = 10 are studied by Ding and Aidun¹³ and Liu et al.³⁰ via a LBM, respectively. As reported in their work, when Re increases to and above a critical Reynolds number Rec, the elliptical solid particle and the elliptical porous particles with $10^{-6} \le Da \le 2 \times 10^{-2}$, cease to rotate and stay at a stationary orientation in the shear flow. When Re is smaller than Re_c , the elliptical particles exhibit time-periodic rotational behavior with a non-uniform angular velocity associated with the orientation of elliptical particles in the simple shear flow. In other words, in a rotation period, the rotation rates of those elliptical particles go through minimum and maximum values. In this work, we further study the rotation of elliptical porous particles based on particle shear Reynolds number Re, dimensionless permeability Da, confinement ratio B, and aspect ratio AR, where we mainly focus on the effects of B. Various confinement ratios B $(=\frac{H}{D}, 2-12)$ and aspect ratios $AR (=\frac{a}{b}, 2-3.5)$ are considered where Da is ranging from 10^{-6} to 10^{-1} and Re is up to 80. The neutrally buoyant elliptical porous particle is initially placed in the geometric center of the rectangular computational domain where the major axis direction is perpendicular to the direction of the shear flow. Although there are no constraints on the motion of the elliptical particle, the center of the neutrally buoyant ellipse is found to remain at its initial position with no translational motion in all simulations. The semi-minor axis of the elliptical particle is set to $b=0.04\,\mathrm{cm}$, and the semi-major axis a can be calculated via a=AR*b.

Basically, the time step is defined as $\delta t_p = \nu/\nu_p * \delta x_p^2$ according to the unit conversion of LBM. Here, ν is the fluid viscosity in the

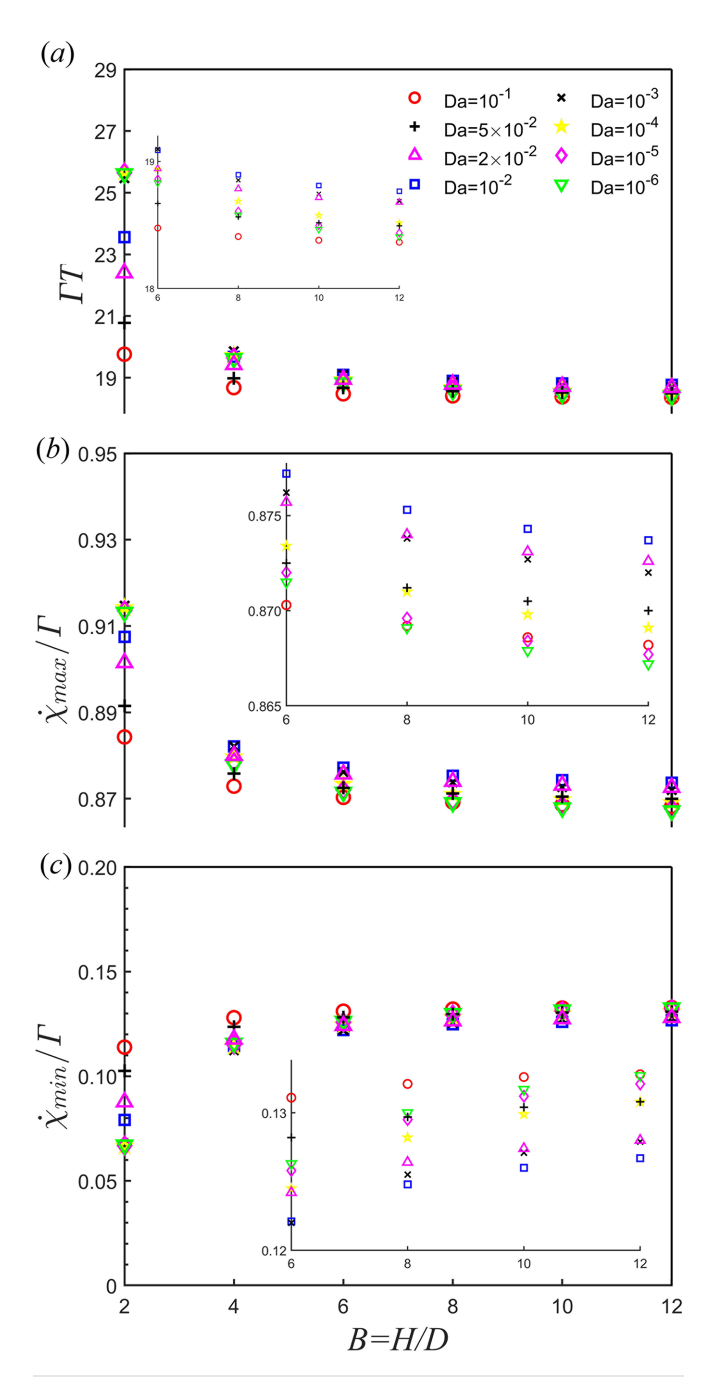


FIG. 4. Dimensionless rotation period ΓT (a), the maximum angular rate $\dot{\chi}_{\rm max}/\Gamma$ (b) and the minimum angular rate $\dot{\chi}_{\rm min}/\Gamma$ (c), as a function of confinement ratio B for elliptical porous particles with AR=2.5 and various Da at Re=0.08. The zoomed-in views of the region $B\geq 6$ are shown.

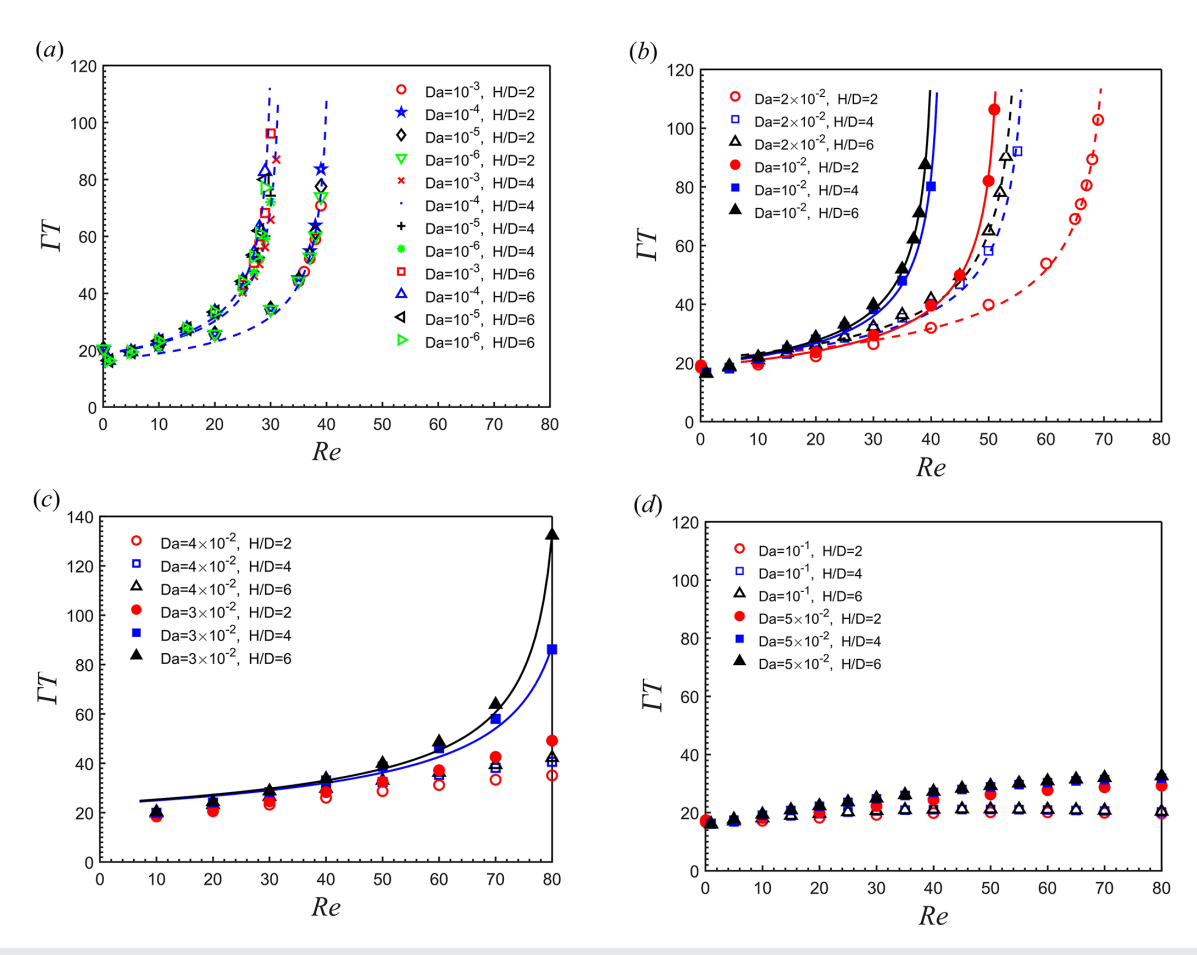


FIG. 5. The dimensionless rotation period ΓT as a function of Re for elliptical porous particles (AR=2) with different confinement ratios (B=2,4,6) and various Da: (a) Da from 10^{-6} to 10^{-3} , (b) Da of 10^{-2} and 10^{-2} and 10^{-2} , (c) Da of 10^{-2} and 10^{-2} , and (d) Da of 10^{-2} and 10^{-1} . The lines are obtained from fitting simulation data with $\Gamma T=C(Re_c-Re)^{-1/2}$.

lattice Boltzmann system, ν_p is the physical fluid viscosity, and δx_p is the physical lattice size. The time step δt_p is for the entire computational domain, which, however, should satisfy the time step requirement for both the pure flow outside the particle and that for flow inside the porous particle. In our simulations, ν_p is fixed at 0.01 cm²/s, δx_p is fixed at 1/360 cm, and $\nu = (\tau - 0.5)/3$ where τ is the relaxation time. It is well established that the stability of LBM for simulating porous media strongly depends on the relaxation time. The relaxation time τ is not fixed for different test cases. In spite of the relaxation time independency, the choice of τ is based on the comprehensive consideration of fluid incompressibility and numerical stability. It is shown that the relaxation time independency is crucial to ensuring the reliable simulation results. We have investigated the independency of τ by checking the rotational parameters including dimensionless rotation period ΓT , dimensionless maximum angular rate $\frac{\chi_{\text{max}}}{\Gamma}$, and minimum angular rate $\dot{\chi}_{\rm min}/\Gamma$ in the current work. In all simulations in this work, τ is found in the range of 0.6–0.8. The independency of the channel width W was checked against the dimensionless rotation period ΓT , dimensionless maximum angular rate $\frac{\chi_{\text{max}}}{\Gamma}$, and minimum angular rate $\dot{\chi}_{\text{min}}/\Gamma$. In this work, we show that W = 20 * 2a is enough to neglect the effects of the channel width when period boundary conditions are used at the two ends of the channel.

A. The effect of B on the rotation without fluid inertia

First, we investigate the confinement effects on the rotation period of the elliptical porous particle at a near-zero Re (Re = 0.08) where the fluid inertia is negligible. A half rotation period is obtained by

TABLE II. The fitting parameters C and Re_c for the scaling law shown in Eq. (10) for the elliptical porous particles with AR=2, $10^{-6} \le Da \le 2 \times 10^{-2}$, and B=2, 4, 6.

Da	B = H/D	C	Re_c
$10^{-6} \sim 10^{-3}$	2	105.11	40.95
	4	106.11	31.93
	6	103.91	30.71
10^{-2}	2	136.99	52.68
	4	126.19	42.31
	6	126.68	41.11
2×10^{-2}	2	179.29	72.00
	4	156.93	57.62
	6	158.03	56.04

calculating the time change when the two adjacent minimum angular rates appear. Figure 4(a) shows the dimensionless rotation period ΓT as a function of the confinement ratio B for elliptical porous particles with a fixed aspect ratio AR = 2.5 and $10^{-6} \le Da \le 10^{-1}$ at Re = 0.08. As can be seen, for each Da studied, ΓT decreases with B and converges to approximately 18.40 when $B \ge 6$. For the small confinement ratios B (< 6), where the confinement plays an important role, the dimensionless rotation period ΓT for the elliptical porous particle decreases with Da monotonously. For example, at B = 2, we obtain $\Gamma T = 19.76$ for $Da = 10^{-1}$ and 25.62 for $Da = 10^{-6}$, where ΓT for $Da = 10^{-1}$ is about 23% lower than that for $Da = 10^{-6}$. This suggests that the permeability affects the rotation period of the elliptical porous particle when the confinement effect cannot be neglected, even if the fluid inertia is negligible. This observation supports the results by Li et al. for circular porous particles.²⁷ For the large confinement ratios $B (\geq 6)$, where the confinement has little effect, the dimensionless rotation period ΓT is around 18.40 and remains almost constant for Da ranging from 10^{-6} to 10^{-1} , which is in good agreement with the analytical solutions for solid impermeable particles ($\Gamma T = 18.22$ for the solid particle with an aspect ratio of 2.5) proposed by Jeffery. This confirms that the permeability has little effect on the rotation of an elliptical porous particle in an unbounded simple shear flow at vanishing Re, which is consistent with the results for ellipsoids concluded by Masoud $et \ al.^{25}$ and for circular porous particles by Li $et \ al.^{27}$

As shown in Fig. 4(a), for porous particles without fluid inertia, the confinement effects are related to Da, which is one of the major features differing from the solid particle. This can also be qualitatively explained. As mentioned, the streamlines which penetrate the particle reduce the contribution from the recirculating region to the particle rotation.²⁷ Balance between the negative and positive torque determines the rotational motion of the porous particle. The change of Da is certainly related to the fluid flow penetrates and goes through the porous particle. It is easy to consider the effects of Da by considering two extreme cases. In one extreme, Da is negligibly small, and the particle can be simplified as a solid impermeable one. In this case, the fluid going through the particle can be neglected, and the enhanced confinement effects (for B decreasing from 6) can significantly promote the rotation period. In another extreme, Da is large enough so that the fluid going through the particle can be significant and the recirculating flow regions would be greatly reduced. The rotation period is increased to a much less extent compared to that for lower Da with the same degree of confinement (for B decreasing from 6).

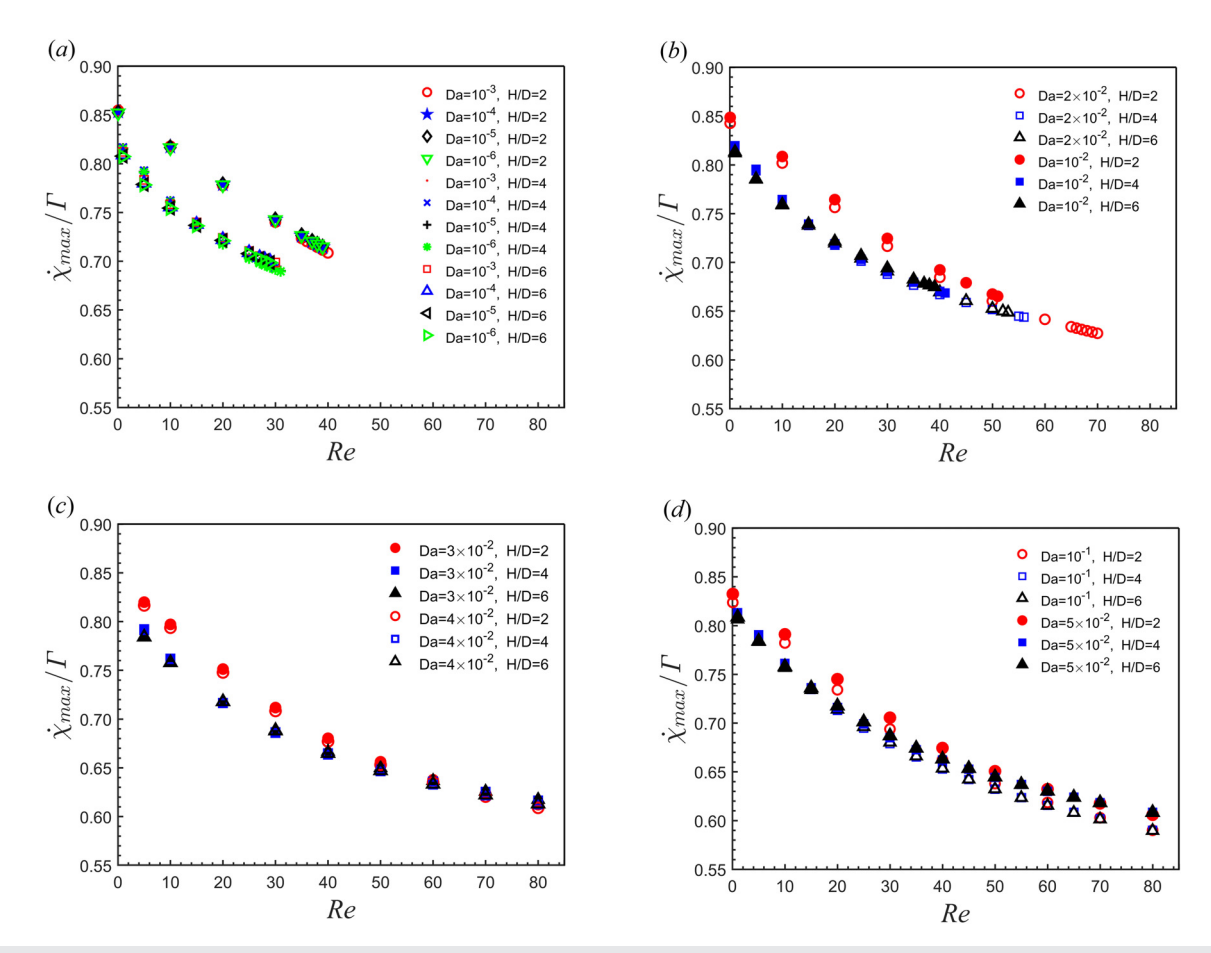


FIG. 6. The maximum angular rate $\dot{\chi}_{\text{max}}/\Gamma$ as a function of Re for elliptical porous particles (AR=2) with different confinement ratios (B=2, 4, and 6) and various Da: (a) small Da from 10^{-6} to 10^{-3} , (b) Da of 10^{-2} and 2×10^{-2} , (c) Da of 3×10^{-2} and 4×10^{-2} , and (d) Da of 5×10^{-2} and 10^{-1} .

For an intermediate Da, however, the combinational effect of confinement and Da works. This briefly explains the results in Fig. 4(a). However, a more accurate theory is highly desired to understand the rotation of porous particle.

As two characteristic rotational rates, the maximum and minimum angular rates are important to reveal the rotational behaviors. Following the effects of B on the rotation period at near-zero Re, the effects of confinement ratio B on the maximum and minimum angular rates for elliptical porous particles with AR = 2.5 and various Da at Re = 0.08 are further examined. As shown in Figs. 4(b) and 4(c), for $B \le 8$, the maximum angular rate $\dot{\chi}_{\rm max}/\Gamma$ decreases and the minimum angular rate $\dot{\chi}_{\rm min}/\Gamma$ increases with the confinement ratio B to various extents, dependent on Da of the elliptical porous particle, i.e., the variation in angular rate within a rotation period decreases with B to various extents, dependent upon Da used. The more permeable the elliptical porous particle, the smaller the variation in angular rate over a period of rotation at a fixed $B \le 8$). For example, at B = 2, the variation range of angular rate within a rotation period is 0.770 for Da = 10^{-1} and 0.846 for $Da = 10^{-6}$, whereas for $B \ge 8$, where the effect of flow confinement is negligible, both $\dot{\chi}_{max}/\Gamma$ and $\dot{\chi}_{min}/\Gamma$ converge to a constant with the increase in B for elliptical porous particles with Da ranging from 10^{-6} to 10^{-1} , further confirming Masoud's²⁵ and Li's²⁷ conclusion that the permeability has little effect on the rotation of the elliptical porous particle in an unbounded simple shear flow in the absence of fluid inertia.

B. The effect of B on the rotation with fluid inertia

In this part, we investigate the effects of confinement ratio B with fluid inertia on the rotational behaviors for elliptical porous particles with two different aspect ratios AR, i.e., AR = 2 and AR = 2.5. By comparing the results for AR = 2 and that for AR = 2.5, the effects of the particle aspect ratio can also be studied briefly.

We first investigate the effects of confinement ratio B with fluid inertia where Re is up to 80 and particle aspect ratio AR=2. Figure 5 shows the dimensionless rotation period ΓT as a function of Re for elliptical porous particles with a fixed AR=2 and various Da ($10^{-6} \leq Da \leq 10^{-1}$) where the confinement ratio B=2, 4, and 6. More results for B=3 and 5 are shown in Appendix B. ΓT and the variation of ΓT vs Re are affected by B to various extents, dependent on Da of the elliptical porous particle used. For particles with Da ranging from 10^{-6} to 4×10^{-2} , as shown in Figs. 5(a)-5(c), ΓT increases with the confinement ratio B when Re>5. Additionally, ΓT increases more

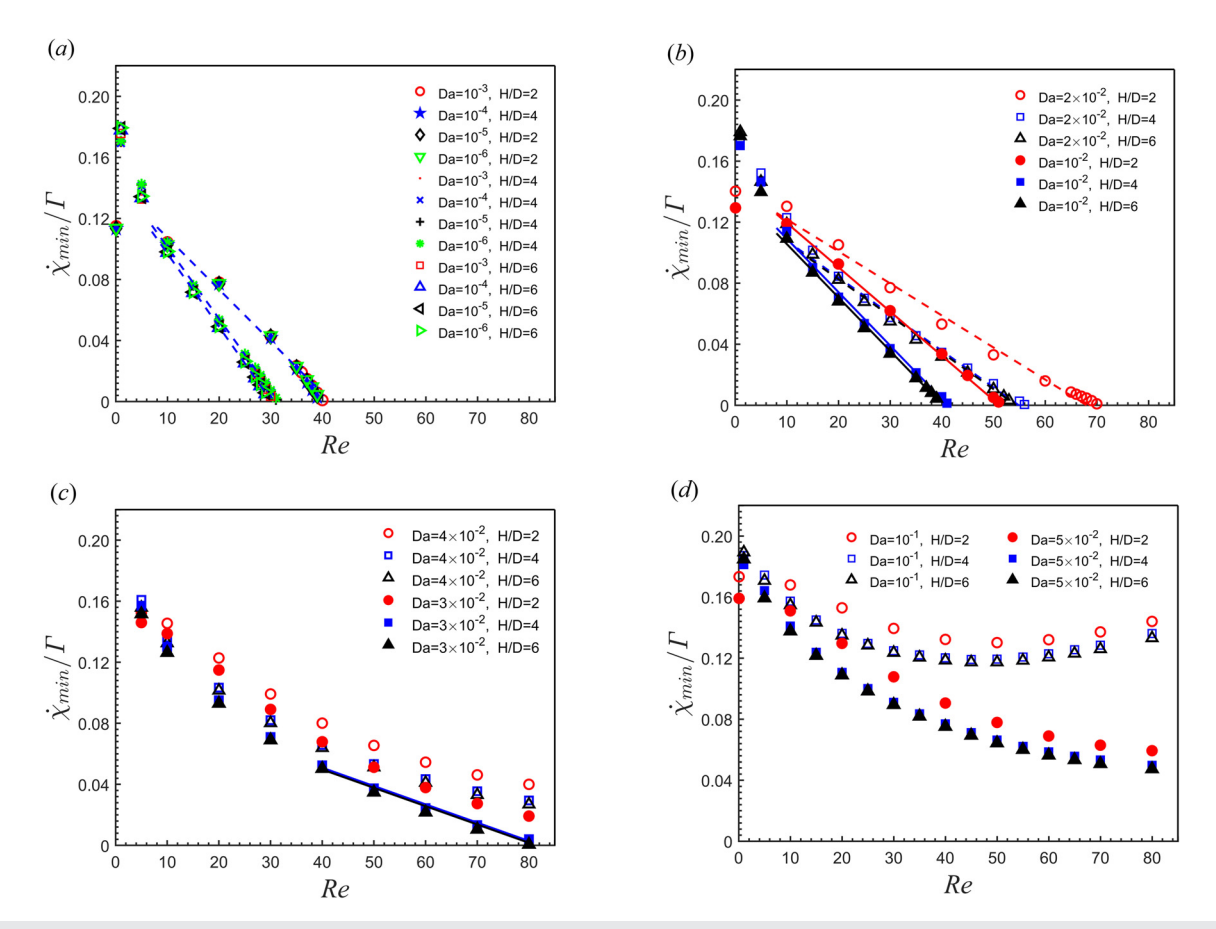


FIG. 7. The minimum angular rate $\dot{\chi}_{min}/\Gamma$ as a function of Re for elliptical porous particles (AR=2) with different confinement ratios (B=2,4, and 6) and various Da: (a) small Da from 10^{-6} to 10^{-3} , (b) Da of 10^{-2} and 2×10^{-2} , (c) Da of 3×10^{-2} and 4×10^{-2} , and (d) Da of 5×10^{-2} and 10^{-1} . The lines show the linear relationship between the minimum angular rate $\dot{\chi}_{min}/\Gamma$ and Re.

rapidly with Re when the confinement ratio B(=H/D) increases from 2 to 6. Therefore, the critical Reynolds number Re_c of the less confined particle is smaller. This phenomenon is similar to that for the solid impermeable elliptical particle reported by Zettner and Yoda¹⁸ and Huang $et\ al.^{15}$ In the meantime, we found that the scaling law

$$\Gamma T = C(Re_c - Re)^{-1/2},\tag{10}$$

which is originally proposed for the solid impermeable elliptical particle 13 and then extended to the elliptical porous particle $(10^{-6} \le Da \le 2 \times 10^{-2})$ in an unbounded simple shear flow, 30 can also be used to describe the relation between ΓT and Re for elliptical particles with AR=2 and $10^{-6} \le Da \le 2 \times 10^{-2}$ in a bounded shear flow where the confinement ratio B=2, 4, 6. In other words, the scaling law is independent of the confinement ratio for elliptical porous particles with AR=2 and $10^{-6} \le Da \le 2 \times 10^{-2}$. In particular, for particles with small Da varying from 10^{-6} to 10^{-3} , the curves of ΓT vs Re nearly overlap, indicating that the permeability has little effect on the rotation period with finite fluid inertia in the bounded simple shear flow, similar to the cases in an unbounded simple shear flow. 30 Thus, we take the data of rotation period vs Re for small Da $(10^{-6} \le Da \le 10^{-3})$ as a whole to fit with the scaling law here. The

two fitting parameters C and Re_c are obtained by fitting the relation between ΓT and Re with the scaling law $\Gamma T = C(Re_c - Re)^{-1/2}$ by the least squares method. The values of C and Re_c for elliptical porous particles with AR = 2 and $10^{-6} \le Da \le 2 \times 10^{-2}$ and three different confinement ratios (B = 2, 4, and 6) are listed in Table II. As depicted in Table II, the values of Re_c get smaller with the increase in the confinement ratio B for elliptical porous particles with $10^{-6} \le Da$ $\leq 2 \times 10^{-2}$. In addition, for $10^{-6} \leq Da \leq 2 \times 10^{-2}$, the curves of ΓT vs Re are practically overlapping when the confinement ratio B varies from 4 to 6, suggesting that the confinement has an almost negligible effect when $B \ge 4$, which is further confirmed by the fitting values of C and Rec listed in Table II. For the elliptical porous particle with $5 \times 10^{-2} \le Da \le 10^{-1}$, as presented in Fig. 5(d), ΓT increases only slightly with B when Re > 5, meaning that the confinement has a minor effect on the rotation period of these particles in the presence of finite fluid inertia. Besides, the increasing rates of dimensionless rotation period ΓT vs Re are almost the same for porous particles with different confinement ratios from 2 to 6.

Following the effects of confinement ratio B on the rotation period with Re up to 80 and AR = 2, the effects of B on the maximum

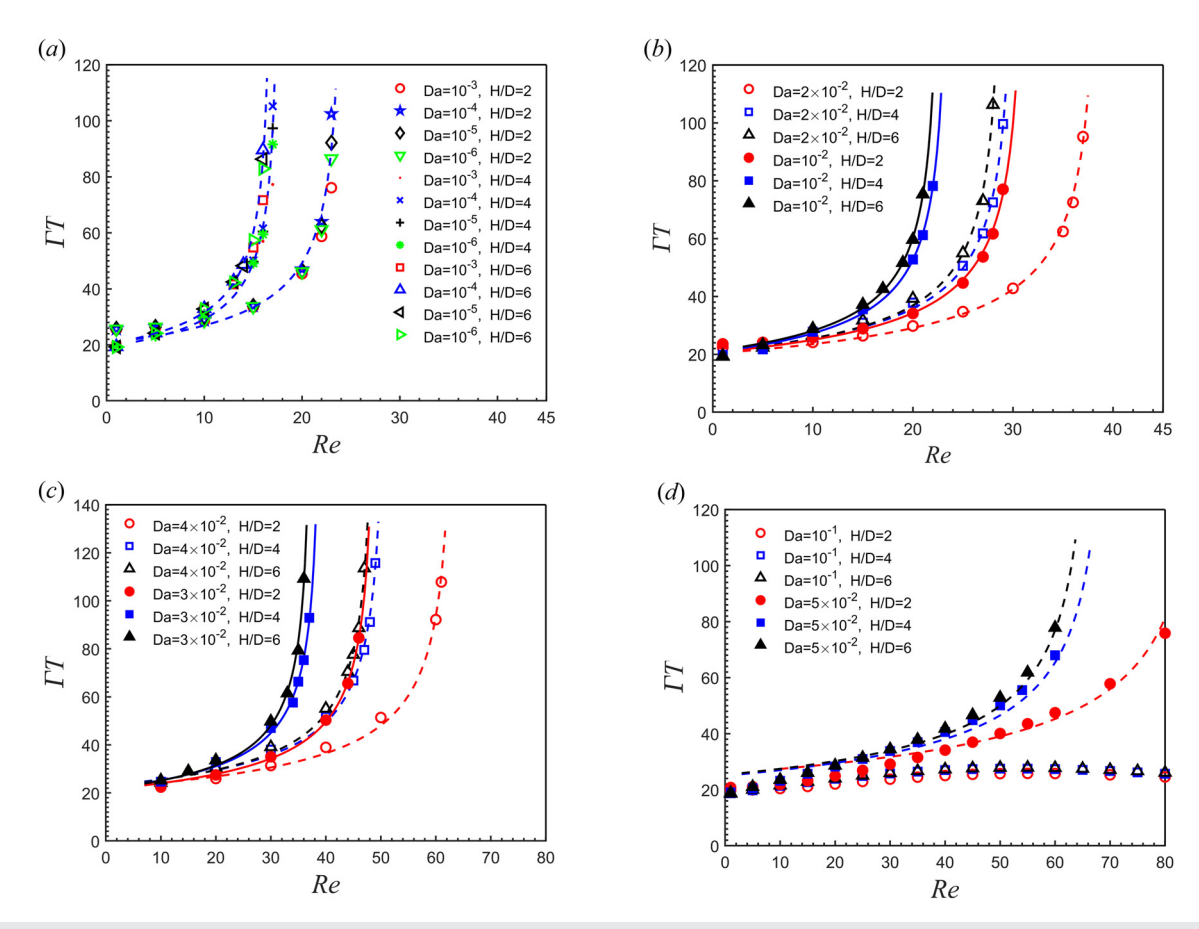


FIG. 8. The dimensionless rotation period ΓT as a function of Re for elliptical porous particles (AR=2.5) with different confinement ratios (B=2,4, and 6) and various Da: (a) small Da from 10^{-6} to 10^{-3} , (b) Da of 10^{-2} and 10^{-2} , (c) Da of 10^{-2} and 10^{-2} , and (d) Da of 10^{-2} and 10^{-1} . The lines are obtained from fitting simulation data with $\Gamma T=C(Re_c-Re)^{-1/2}$.

and minimum angular rates are further studied. Figures 6 and 7 show the maximum angular rate $\dot{\chi}_{\rm max}/\Gamma$ and the minimum angular rate $\dot{\chi}_{\rm min}/\Gamma$, respectively, as a function of Re for elliptical porous particles (AR = 2) with various Da ($10^{-6} \le Da \le 10^{-1}$) and different confinement ratios B (B = 2, 4, 6) where Re is up to 80. As can be seen in both Figs. 6 and 7, for the whole range of Da, the curves of both $\dot{\chi}_{\rm max}/\Gamma$ and $\dot{\chi}_{\rm min}/\Gamma$ vs *Re* overlap when the confinement ratio $B \ge 4$, indicating that the effect of confinement is negligible when B increases to beyond 4. Whereas when $B \le 4$, as shown in Figs. 6(a)-6(d), the maximum angular rate $\dot{\chi}_{\rm max}/\Gamma$ decreases with the increase in confinement ratio B, and the decreasing rate becomes smaller with the increase in Re and Da. The variation of $\dot{\chi}_{\rm max}/\Gamma$ vs B for elliptical porous particles with $10^{-6} \le Da \le 10^{-1}$ shows the same trend as that for the solid impermeable elliptical particle reported by Zettner and Yoda. 18 As shown in Figs. 7(a) and 7(b), for elliptical porous particles with $10^{-6} \le Da \le 2 \times 10^{-2}$ in a bounded simple shear flow, the minimum angular rate $\dot{\chi}_{min}/\Gamma$ decays linearly down to 0 for intermediate Re, and the decaying rate increases with B. This suggests that the more confined elliptical porous particle exhibits a larger critical Reynolds number Re_c where $\dot{\chi}_{\min}/\Gamma$ is 0, which is consistent with the results of Figs. 5(a) and 5(b). It is noteworthy that, when the Re approaches Re_c , the dimensionless minimum angular rate $\dot{\chi}_{\min}/\Gamma$ will reduce to zero, and meanwhile, the dimensionless rotation period ΓT will increase to infinite. Therefore, Re_c can be predicted based on either the minimum angular rate approaching zero or fitting the dimensionless rotation period ΓT as a function of Re using formula shown by Eq. (10). Moreover, for the whole range of Da when $B \leq 4$, as shown in Fig. 7, $\dot{\chi}_{\rm min}/\Gamma$ decreases with B for $Re \geq 5$. The variation trend of $\dot{\chi}_{\rm min}/\Gamma$ vs B for intermediate Re is similar to the solid impermeable elliptical particles.

The effects of B on the rotational behaviors of elliptical porous particles with AR = 2.5 and Re up to 80 are then examined. The dimensionless rotation periods ΓT as a function of Re for elliptical porous particles with a fixed AR = 2.5 where the confinement ratio B = 2, 4, 6 are presented in Fig. 8. More results for B = 3 and 5 are shown in Appendix B. As illustrated in Figs. 8(a)-8(d), for elliptical porous particles with $10^{-6} \le Da \le 5 \times 10^{-2}$ and AR = 2.5 in a bounded simple shear flow, the scaling law [Eq. (10)] can also be used to describe the relation between ΓT and Re. The values of C and Re_c for AR = 2.5 fitted by the scaling law are listed in Table III. By comparing Figs. 8 and 5, we find that the effects of B on the rotation period of elliptical porous particles with AR = 2.5 are qualitatively similar to that of AR = 2. Additionally, comparison between Figs. 8 and 5 also shows that ΓT increases with AR and ΓT shows a more rapid increase with Re for larger aspect ratio AR, resulting in a smaller Re_c . This trend is consistent with the observations by Huang et al. 15 and Zettner and Yoda 18 for the solid impermeable elliptical particle. Furthermore, the comparison between Figs. 8 and 5 also suggests that the scaling law is independent of the aspect ratio of elliptical porous particles in a bounded simple shear flow. As conjectured by Ding and Aidun¹³ in their numerical simulations and then confirmed by Zettner and Yoda¹⁸ in their experiments, the scaling law is independent of the particle aspect ratios for the solid elliptical particle. Comparison between Tables II and III shows that the larger the AR, the smaller the Re_c (if observed). For example, for $Da = 10^{-2}$ and B = 2, we obtain $Re_c = 52.68$ for AR = 2 and $Re_c = 31.35$ for AR = 2.5. It is

TABLE III. The fitting parameters *C* and Re_c for the scaling law shown in Eq. (10) for the elliptical porous particles with AR=2.5, $10^{-6} \le Da \le 5 \times 10^{-2}$, and B=2,4, and 6.

Da	B = H/D	C	Re_c
$10^{-6} \sim 10^{-3}$	2	101.81	24.28
	4	81.00	17.70
	6	83.40	16.93
10^{-2}	2	115.49	31.35
	4	100.71	23.66
	6	100.67	22.79
2×10^{-2}	2	126.27	38.83
	4	115.34	30.37
	6	111.45	29.12
3×10^{-2}	2	150.29	49.17
	4	136.35	39.20
	6	131.81	37.50
4×10^{-2}	2	177.23	63.58
	4	164.21	51.07
	6	159.26	49.04
$5 imes 10^{-2}$	2	231.58	88.78
	4	214.56	70.81
	6	200.36	66.95

worth mentioning that for elliptical porous particles with $Da = 5 \times 10^{-2}$ and AR = 2.5, as shown in Fig. 8(d), the relation between ΓT and Re can be well fitted with the scaling law, demonstrating that the scaling law may be applicable to particles with high permeability as long as the range of Re is wide enough.

We further investigate the effect of confinement ratio B on the maximum and minimum angular rates with AR = 2.5 and Reup to 80. Figures 9 and 10 show, respectively, the maximum angular rate $\dot{\chi}_{\rm max}/\Gamma$ and the minimum angular rate $\dot{\chi}_{\rm min}/\Gamma$ as a function of Re for elliptical porous particles with a fixed AR = 2.5 and three confinement ratios B (B = 2, 4, 6). Comparisons between Figs. 9 and 6, Figs. 10 and 7, show that the effects of confinement ratio B on $\dot{\chi}_{\rm max}/\Gamma$ and $\dot{\chi}_{\rm min}/\Gamma$ for elliptical porous particles with AR = 2.5 are similar to those for AR = 2. In addition, by comparing Figs. 9 and 6, Figs. 10 and 7, we find that for the whole range of $\it Da$ and $\it Re, \, \dot{\chi}_{\rm max}/\Gamma$ increases and $\dot{\chi}_{\rm min}/\Gamma$ decreases as the aspect ratio AR increases. That is, the variation in angular rate within a rotation period increases with the aspect ratio. Specifically, for elliptical particles with $Da~(10^{-6} \le Da \le 5 \times 10^{-2})$, as shown in Fig. 10, the minimum angular rate $\dot{\chi}_{min}/\Gamma$ decreases linearly to 0 with *Re* for intermediate *Re*.

C. The effect of B on the critical Reynolds number Re_c

As pointed above, the elliptical porous particles exhibit a transition (if observed) from rotating to stationary when Re is above a critical Reynolds number Re_c . Different from Re_c , Re_{cr} is the numerical simulated critical Reynolds number which we obtain by gradually increasing Re with the increment step of 1 until the particle stops rotating, which is used to validate the accuracy of the fitting Re_c . The values of Re_{cr} for elliptical porous particles at different confinement

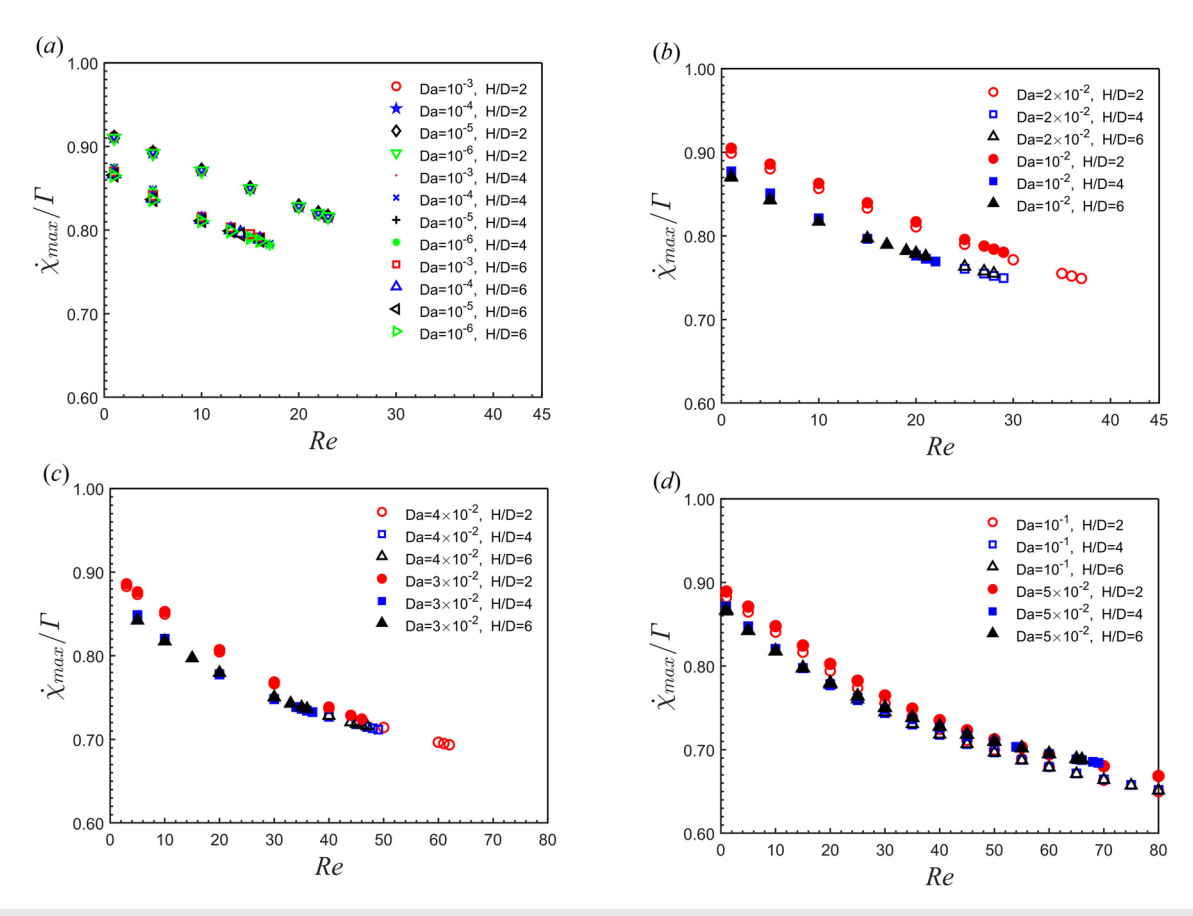


FIG. 9. The maximum angular rate $\dot{\chi}_{\text{max}}/\Gamma$ as a function of Re for elliptical porous particles (AR=2.5) with different confinement ratios (B=2, 4, and 6) and various Da: (a) small Da from 10^{-6} to 10^{-3} , (b) Da of 10^{-2} and 10^{-2} , (c) Da of 10^{-2} and 10^{-2} , and (d) Da of 10^{-2} and 10^{-1} .

ratios B with various Da ($10^{-6} \le Da \le 2 \times 10^{-2}$) and aspect ratios AR are shown in detail in Figs. 11(a)-11(c). From these figures, we find that for all AR and Da studied here, Re_{cr} decreases with confinement ratio B and remains nearly constant when $B \ge 6$. In particular, for Da ranging from 10^{-6} to 10^{-3} , the variations of Re_{cr} vs B are almost overlapping with each other, indicating that the permeability has little effects on Re_{cr} in this case. At a fixed B, the Re_{cr} decreases with the increase in a Re_{cr} in this case. At a fixed Re_{cr} decreases with the increase in Re_{cr} in this case. At a fixed Re_{cr} decreases with the increase in Re_{cr} and Re_{cr} = 21 for Re_{cr} = 38 for Re_{cr} = 25, and Re_{cr} = 27 for Re_{cr} = 3. Besides, the values of Re_{cr} predicted by the scaling law shown in Tables II and III are very close to Re_{cr} obtained by our simulations presented in Figs. 11(a) and 11(b), further confirming that the scaling law is valid for the elliptical porous particle with various aspect ratios in a bounded shear flow.

To quantitatively describe the effects of confinement ratio B and aspect ratio AR together with dimensionless permeability Da on the critical Reynolds number Re_c , we proposed an empirical formula to correlate Re_c as a function of B, AR, and Da by symbolic regression. Symbolic regression is a method based on evolutionary computation³⁴ and aims to find a mathematical model and minimize various error metrics³⁵ from input data. Compared with other data-driven machine learning methods, symbolic regression can search parameters and the functional form of the model simultaneously³⁵ without any

assumptions. The initial expression of the model is composed of various building blocks, including algebraic operators, trigonometric function, and so on. After calculation, the algorithm returns the most accurate equations at a certain complexity. Symbolic regression has been widely used to extract models based on input data for many systems. 36,37 The training data to correlate Re_c as a function of B, AR, and Da are listed in Table IV. It is noted that the data for the case of B=H/D=10 where the effects of confinement can be completely neglected 30 is also included as input data in order to improve the accuracy of the final expression. An empirical formula of Re_c as a function of AR, B, and Da is obtained by symbolic regression

$$Re_c = 210.5 Da + \frac{22.59}{B} + \frac{39.16}{AR - 18.13 Da - 1.002} - 12.93.$$
 (11)

The correlation coefficient (*CC*) and mean squared error (*MSE*) are used to evaluate the accuracy of this formula. This shown that CC = 0.997 and MSE = 1.996 for the training data sets. We conduct another set of extra simulations for AR = 3.5 which is used as a test case to further evaluate the availability of this formula. The results for AR = 3.5 are shown in Table V in the following. CC = 0.992 and MSE = 1.345 could be obtained for the test data set, indicating the satisfactory accuracy of the formula. We stress that the proposed formula can present a better prediction of Re_c for elliptical porous particles

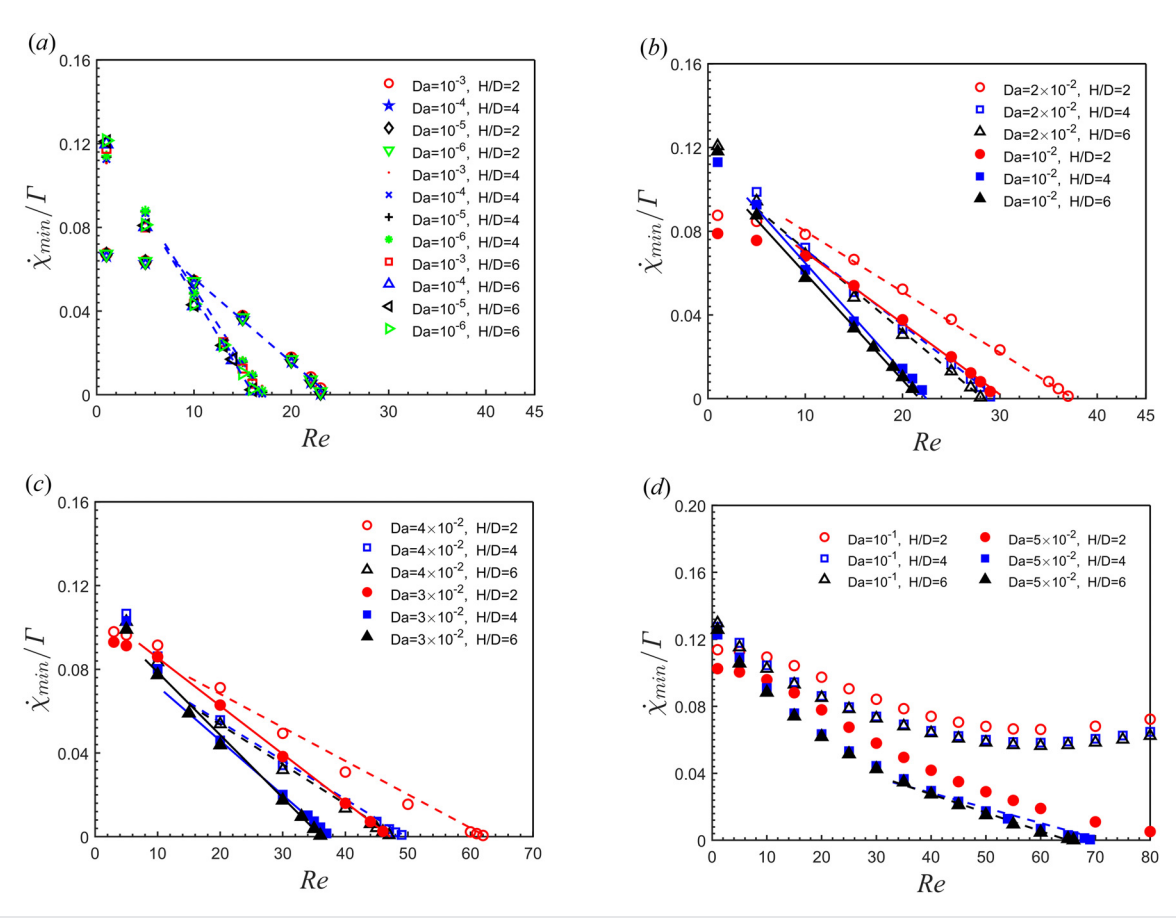


FIG. 10. The minimum angular rate $\dot{\chi}_{min}/\Gamma$ as a function of Re for elliptical porous particles (AR=2.5) with different confinement ratios (B=2,4, and 6) and various Da: (a) small Da from 10^{-6} to 10^{-3} , (b) Da of 10^{-2} and 2×10^{-2} , (c) Da of 3×10^{-2} and 4×10^{-2} , and (d) Da of 5×10^{-2} and 10^{-1} . The lines show the linear relationship between the minimum angular rate $\dot{\chi}_{min}/\Gamma$ and Re.

with aspect ratios from 2 to 3.5. For the aspect ratio beyond this range, however, it requires further validation.

D. The surrounding flow field and net torque acting on the elliptical porous particle

To better understand the flow field around the elliptical porous particle, we also check the flow patterns and the pressure distribution. Figure 12 shows typical flow patterns for elliptical porous particles freely rotating in a simple shear flow with different confinement ratios B and aspect ratios AR where the pressure distribution is shown as well. The pressure p is computed as $p = \rho c_s^2$ in LBM simulations. Note that ρ is the density of fluid and the lattice sound speed $c_s = 1/\sqrt{3}$. Hence, the normalized pressure can be estimated by $p' = p/(\rho_0/3)$ with ρ_0 the initial density of the fluid. As illustrated in Fig. 12, the whole flow field can be divided into five regions by streamlines. Two shear flow regions above and below the particle, which are essentially caused by the fluid flow adjacent to the two bounding walls moving along the opposite directions, and these two shear flow regions, contribute positive torque to the particle rotation. Two recirculating flow regions on the left and right of the particle contribute negative

torque on the particle rotation. A fluid layer moving near and around the particle at the surface can penetrate through the particle. The streamlines which penetrate the particle reduce the contribution from the recirculating regions to the particle rotation.²⁷ When the negative torque balances the positive torque, the elliptical porous particle stops rotating. The flow patterns outside the elliptical porous particle with various aspect ratios freely rotating in a confined simple shear flow are similar to those of solid impermeable particles,¹⁸ and both have the fluid flow adjacent to the two bounding walls moving along the opposite directions and the recirculation of fluid flow in the middle of the channel

Additionally, one interesting phenomenon observed is that for elliptical porous particles with small permeability $(10^{-6} \le Da \le 10^{-3})$, two small vortices appear to the left and right of the horizontal particle when Re approaches Re_c , and this phenomenon is independent of the aspect ratio and confinement ratio. Figure 13 shows the contours of streamlines for a horizontal elliptical porous particle freely rotating in a simple shear flow with AR = 2, $Da = 10^{-4}$, B = 6 and various Re, where the pressure distribution is also shown. As can be seen in Fig. 13(a), for Re = 5, the two vortices do not appear, and there exist only two stagnation points. For Re = 15, as shown in Fig. 13(b),

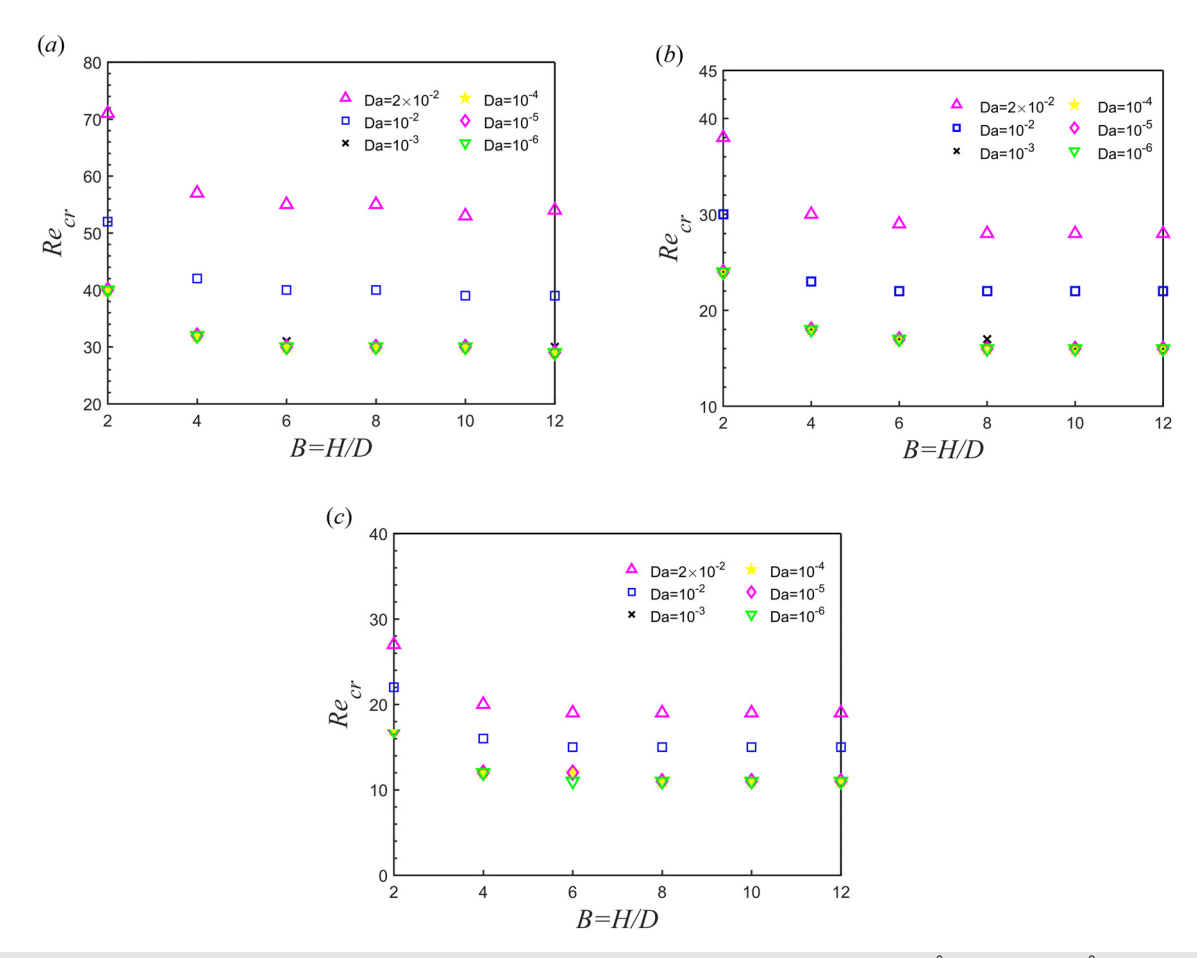


FIG. 11. The critical Reynolds number Re_{cr} as a function of confinement ratio B for elliptical porous particles with various Da ($10^{-6} \le Da \le 2 \times 10^{-2}$) and aspect ratios AR: (a) AR = 2, (b) AR = 2.5, and (c) AR = 3.

the two vortices are observed, and meanwhile, the number of stagnation points increases to 4. The size of the vortices increases with a higher Re. The appearance and evolution of the two vortices are interesting, though the underlying physics might be complex. We anticipate that the formation of the vortices may be related to the fluid flow adjacent to the two bounding walls moving along the opposite directions and the recirculation of fluid flow in the middle of the channel. As shown in our previous work,²⁷ there exists a fluid layer moving near and around the particle at the surface transferring the momentum from the moving walls and the recirculating flow. For the elliptical porous particle, this fluid layer may show an alternative movement. Furthermore, as can be seen from Fig. 13, there exist two highpressure regions and two low-pressure regions near the particle surface. The two small vortices locate in the middle of the high- and lowpressure regions. Therefore, the formation and evolution of the two vortices may be related to the pressure distribution near the surface of the particle. Take the left end of the particle as an example, it is shown that the pressure difference between the high- and low-pressure regions increases with Re. Further increase in the pressure difference at higher Re might cause the vortex shedding alike phenomenon form. This preliminary speculation on the mechanism underlying the

formation of these vortices, however, calls for further work that can deepen our understanding in this regard. For particles with high permeability, the resistance arising from the porous particle is smaller; thus more fluid can penetrate through the particle. Therefore, there is no formation of small vortices for these particles.

Finally, to explain the transition for the elliptical porous particle from rotating to stationary (when observed), we show the net torques for a fixed porous ellipse with orientation angles ranging from 0 to π . The net torque is a dimensionless torque defined as $T_q/\mu\Gamma D^2$, where T_a is calculated via the momentum-change method. Figure 14 shows the net torque exerted on the fixed elliptical porous particles with various aspect ratios AR and dimensionless permeability Da at different Re and confinement ratios B, as a function of orientation angle χ/π , which is normalized by π . As shown in Fig. 14(a) where AR = 2, B= 2, and $Da = 10^{-2}$, when Re = 30, the torque on the fixed elliptical porous particle is always positive when the orientation angle χ/π varies from 0 to 1. Therefore, the elliptical porous particle rotates with the shear flow at Re = 30. This phenomenon has also been observed by Ding and Aidun¹³ for the solid impermeable elliptical particle. When Re increases to 52, as shown in Fig. 14(a), the curve of net torque is just tangent to the χ axis, i.e., there is one fixed point on the

TABLE IV. The values of Re_c obtained from fitting simulation data with the scaling law [Eq. (10)] at various AR, B, and Da.

TABLE IV. (Continued.)

law [Eq. (10)] at various AR, B, and Da.			AD = a/b $D = H/D$ Da Da				
AR = a/b	B = H/D	Da	Re_c	$\frac{AR = a/b}{a}$	B = H/D	Da	Re _c
3	2	5×10^{-2}	48.56	2.5 2.5	3	$10^{-5} \\ 10^{-6}$	19.51 19.60
3	2	4×10^{-2}	39.77	2.5	3 4	5×10^{-2}	70.81
3	2	3×10^{-2}	33.08	2.5	4	4×10^{-2}	51.07
3	2	2×10^{-2}	27.04	2.5	4	3×10^{-2}	39.20
3	2	10^{-2}	22.07	2.5	4	2×10^{-2}	39.20
3	2	10^{-3}	17.78	2.5	4	2×10^{-2}	23.66
3	2	10^{-4}	16.95	2.5		10^{-3}	18.24
3	2	10^{-5}	17.11	2.5	4	10^{-4}	17.58
3	2	10^{-6}	17.25	2.5	4	10^{-5}	17.38
3	4	5×10^{-2}	39.01		4	10^{-6}	
3	4	4×10^{-2}	31.15	2.5	4		17.81
3	4	3×10^{-2}	25.22	2.5	5	5×10^{-2}	68.37
3	4	2×10^{-2}	20.37	2.5	5	4×10^{-2}	49.52
3	4	10^{-2}	16.05	2.5	5	3×10^{-2}	38.39
3	4	10^{-3}	12.26	2.5	5	2×10^{-2}	29.77
3	4	10^{-4}	12.20	2.5	5	10^{-2}	22.50
3	4	10^{-5}	12.36	2.5	5	10^{-3}	17.77
		10^{-6}		2.5	5	10^{-4}	17.27
3	4	5×10^{-2}	12.41 37.29	2.5	5	10^{-5}	17.33
3	6			2.5	5	10^{-6}	17.41
3	6	4×10^{-2}	29.85	2.5	6	5×10^{-2}	66.95
3	6	3×10^{-2}	24.31	2.5	6	4×10^{-2}	49.04
3	6	2×10^{-2}	19.64	2.5	6	3×10^{-2}	37.50
3	6	10^{-2}	15.41	2.5	6	2×10^{-2}	29.12
3	6	10^{-3}	11.72	2.5	6	10^{-2}	22.79
3	6	10^{-4}	11.20	2.5	6	10^{-3}	17.45
3	6	10^{-5}	11.27	2.5	6	10^{-4}	16.86
3	6	10^{-6}	11.34	2.5	6	10^{-5}	16.93
3	10	2×10^{-2}	19.32	2.5	6	10^{-6}	17.01
3	10	10^{-2}	15.16	2.5	10	2×10^{-2}	28.99
3	10	10^{-3}	11.62	2.5	10	10^{-2}	22.14
3	10	10^{-4}	11.30	2.5	10	10^{-3}	16.93
3	10	10^{-5}	11.34	2.5	10	10^{-4}	16.65
3	10	10^{-6}	11.39	2.5	10	10^{-5}	16.70
2.5	2	4×10^{-2}	63.58	2.5	10	10^{-6}	16.76
2.5	2	3×10^{-2}	49.17	2	2	$2 imes 10^{-2}$	72.00
2.5	2	2×10^{-2}	38.83	2	2	10^{-2}	52.68
2.5	2	10^{-2}	31.35	2	2	10^{-3}	40.95
2.5	2	10^{-3}	25.13	2	2	10^{-4}	40.87
2.5	2	10^{-4}	23.95	2	2	10^{-5}	41.27
2.5	2	10^{-5}	24.28	2	2	10^{-6}	41.57
2.5	2	10^{-6}	24.51	2	3	2×10^{-2}	61.73
2.5	3	5×10^{-2}	75.63		3	10^{-2}	45.10
2.5	3	4×10^{-2}	54.10	2			
2.5	3	$3 imes 10^{-2}$	41.38	2	3	10^{-3}	34.40
2.5	3	2×10^{-2}	32.30	2	3	10^{-4}	33.89
2.5	3	10^{-2}	24.84	2	3	10^{-5}	34.08
2.5	3	10^{-3}	19.87	2	3	10^{-6}	34.25
2.5	3	10^{-4}	19.40	2	4	3×10^{-2}	86.24

TABLE IV. (Continued.)

		_	
AR = a/b	B = H/D	Da	Re_c
2	4	2×10^{-2}	57.62
2	4	10^{-2}	42.31
2	4	10^{-3}	32.53
2	4	10^{-4}	31.93
2	4	10^{-5}	31.64
2	4	10^{-6}	31.84
2	5	3×10^{-2}	84.16
2	5	2×10^{-2}	56.75
2	5	10^{-2}	41.43
2	5	10^{-3}	31.77
2	5	10^{-4}	30.67
2	5	10^{-5}	30.82
2	5	10^{-6}	31.01
2	6	3×10^{-2}	82.64
2	6	$2 imes 10^{-2}$	56.04
2	6	10^{-2}	41.11
2	6	10^{-3}	31.18
2	6	10^{-4}	30.58
2	6	10^{-5}	30.71
2	6	10^{-6}	30.85
2	10	$2 imes 10^{-2}$	54.61
2	10	10^{-2}	40.37
2	10	10^{-3}	30.78
2	10	10^{-4}	29.98
2	10	10^{-5}	30.10
2	10	10^{-6}	30.26

TABLE V. The fitting parameters *C* and Re_c for the scaling law shown in Eq. (10) for the elliptical porous particles with AR=3.5, $10^{-6} \le Da \le 5 \times 10^{-2}$, and B=2, 4, and 6.

Da	B = H/D	С	Re_c
$10^{-3} \sim 10^{-6}$	2	112.10	13.23
	4	69.55	9.23
	6	71.93	8.67
10^{-2}	2	114.44	17.55
	4	86.51	12.24
	6	83.87	11.45
2×10^{-2}	2	114.98	21.26
	4	97.09	15.25
	6	92.54	13.39
5×10^{-2}	2	133.60	34.56
	4	130.03	26.87
	6	128.54	26.00

curve where the net torque acting on the porous particle is 0. Here, the net torque is 0 when the orientation angle $\chi/\pi = 0.465$. This means that the elliptical porous particle ceases to rotate and stays stationary at orientation angle $\chi/\pi=0.465$ and Re=52, which is the critical Reynolds number consistent with Fig. 11(a). When Re further increases to 72, as can be seen, there are two fixed points where the net torque is 0. However, only the left fixed point at $\chi/\pi=0.390$ is stable and the orientation of the elliptical porous particle will converge to this fixed point ultimately. The other right fixed point where χ/π = 0.503 is unstable. That is, if the initial orientation angle slightly deviates from $\chi/\pi = 0.503$, the elliptical porous particle will rotate to diverge away from this unstable fixed point and converge to the stable angle $\chi/\pi = 0.390$ in this case. In addition, as presented in Fig. 14(b), the variation trend of the net torque vs χ/π for confinement ratio B=6 is similar to that for B=2 as shown in Fig. 14(a) for elliptical porous particles with AR = 2 and $Da = 10^{-2}$, and the critical Reynolds number decreases from 52 to 40 when B increases from 2 to 6. Comparison between Figs. 14(b) and 14(c) also shows that the variations of net torque are also similar to each other when aspect ratio AR varies from 2 to 3 for particles with B = 6 and $Da = 10^{-2}$, and the critical Reynolds number varies from 40 to 15. However when $Da = 10^{-1}$, AR = 2 and B = 6, as shown in Fig. 14(d), the net torque on the elliptical porous particle for Re up to 80 is always positive; hence the highly permeable particle will not stop rotating. From Figs. 14(a)-14(d), we can conclude that the variation of net torque on the fixed elliptical porous particle vs orientation angle can help to estimate whether the corresponding freely rotating particle ceases to rotate in a simple shear flow, regardless of the aspect ratio and confinement effect. If the particle does stop, the net torque can further help to determine the orientation angle and Reynolds number at which the elliptical porous particle finally stops.

V. CONCLUSIONS

In this study, we investigate the rotation of a neutrally buoyant elliptical porous particle initially placed in the geometric center of a simple shear flow by solving the volume-averaged macroscopic equations by a two-dimensional LBM, focusing on the effects of confinement ratio B. The rotation dynamics of elliptical porous particles with varying aspect ratios AR, Darcy number Da, and Reynolds number Re are examined for different confinement ratios B.

At vanishing Re, our simulation results confirm that the permeability has little effect on the rotational behaviors of elliptical porous particles when the confinement effect is negligible ($B \ge 8$), but also suggest that the effect of permeability cannot be neglected when the role of confinement is important even in the absence of fluid inertia. At finite *Re*, we found that for $B \ge 4$, the confinement has a negligible effect on the rotation of the elliptical porous particle, while for $B \leq 4$, B can alter the dimensionless rotation period ΓT . ΓT increases more rapidly for either larger B or bigger aspect ratio, resulting in a smaller critical Reynolds number Re_c , at which the elliptical porous particle stops rotating. A scaling law initially proposed for elliptical solid particle can be extended to correlate ΓT and Re for the elliptical porous particles, regardless of the effects of B and AR. A larger B causes a reduction of the maximum angular rate $\dot{\chi}_{\rm max}/\Gamma$, and a smaller B meantime leads to an increasing minimum angular rate $\dot{\chi}_{min}/\Gamma$. Furthermore, a higher AR leads to an increase in $\dot{\chi}_{\rm max}/\Gamma$ and a drop in $\dot{\chi}_{\rm min}/\Gamma$.

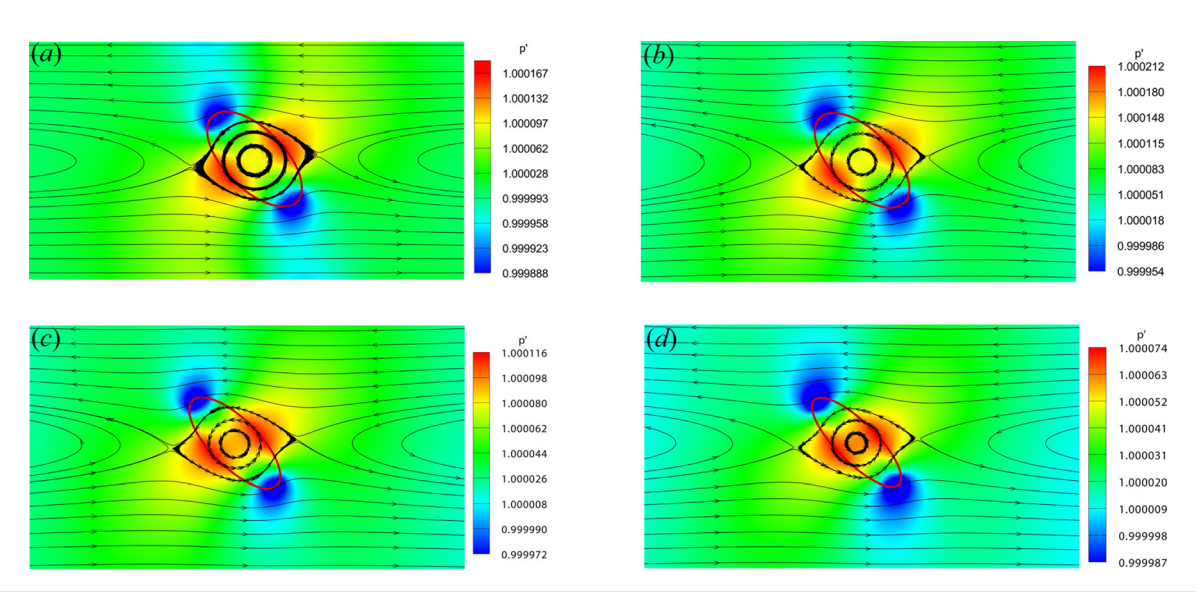


FIG. 12. Flow patterns for elliptical porous particles freely rotating in a simple shear flow with different confinement ratios B and aspect ratios AR: (a) B=2, AR=2, (b) B=6, AR=2, (c) B=6, AR=2.5, and (d) B=6, AR=3. The pressure distribution is given as well. The fixed orientation angle of 0.25π is chosen with R=10 and $R=10^{-2}$.

In order to quantitatively describe the effects of confinement ratio B on critical Reynolds number Re_c at which the elliptical porous particle stops rotating, we proposed an empirical formula to correlate Re_c as a function of B, AR, and Da based on symbolic regression which can simultaneously search parameters and the functional form of the model. The correlation coefficient CC = 0.997 and mean squared error

MSE = 1.996, demonstrating good accuracy of the formula. Additionally, the flow patterns for elliptical porous particles in a simple shear flow are similar to that for solid impermeable elliptical particles, ¹³ independent of confinement ratio B. In general, the flow field can be divided into five regions: two shear flow regions above and below the particle, two recirculating flow regions on the left and right

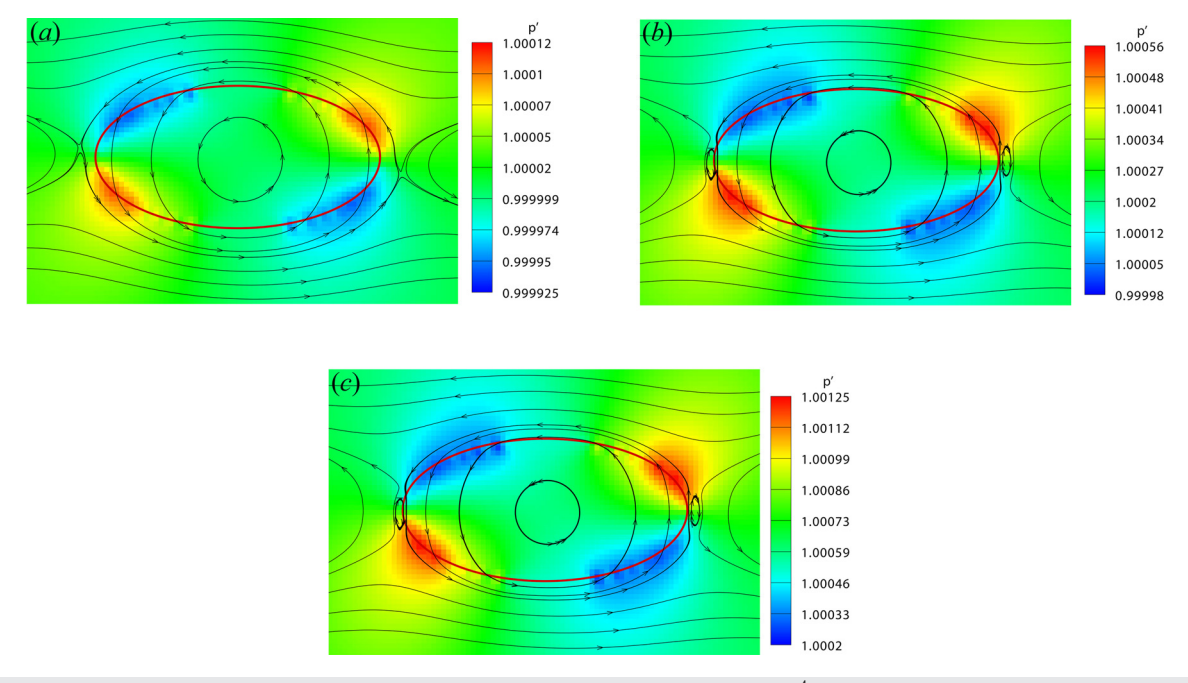


FIG. 13. Streamlines for elliptical porous particles freely rotating in a simple shear flow with AR = 2, $Da = 10^{-4}$, B = 6, and various Re where the pressure distribution is also shown: (a) Re = 5, (b) Re = 15, and (c) Re = 25. The fixed orientation angle of 0.5π is chosen. The critical Reynolds number in this case is $Re_c = 30$.

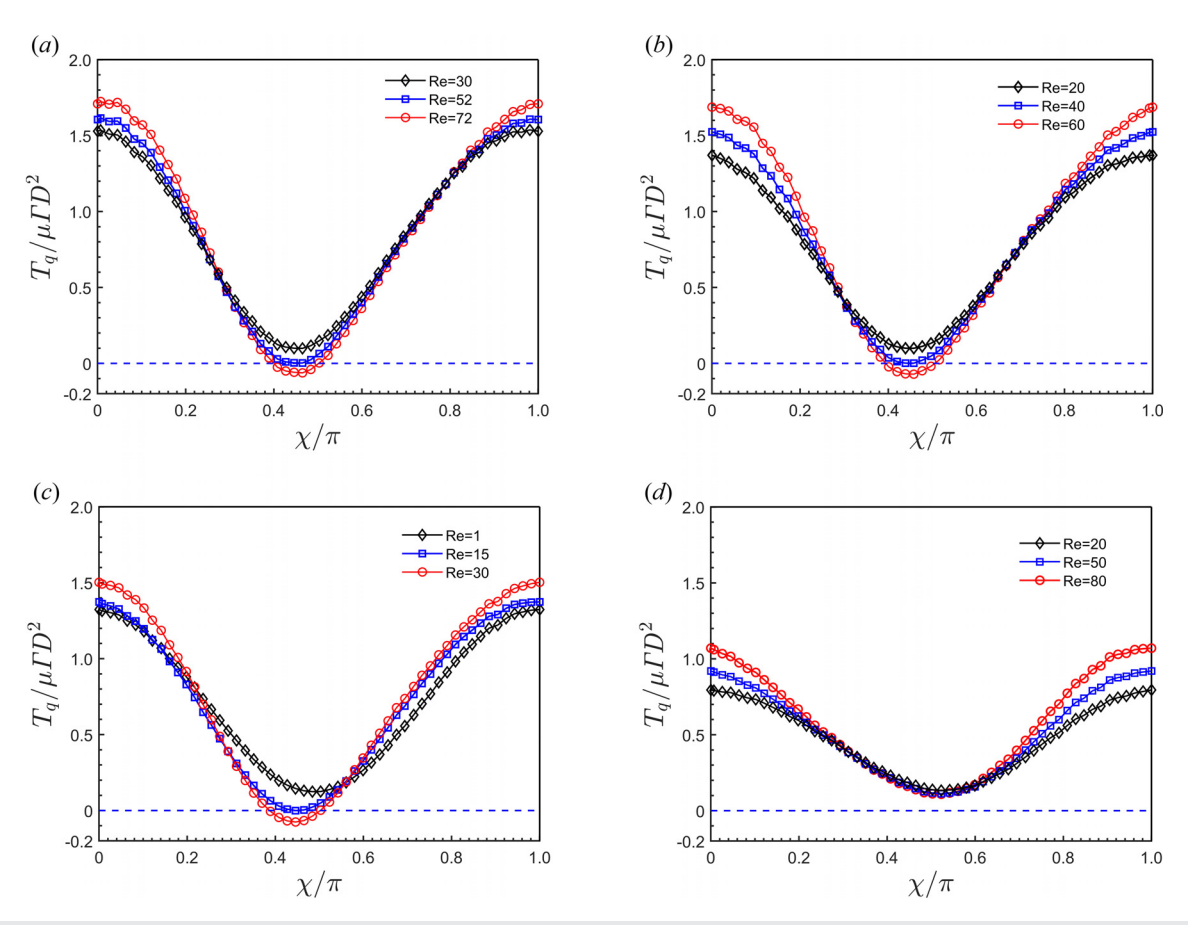


FIG. 14. The net torque acting on the fixed elliptical porous particles by fluid as a function of orientation angle with various AR, B and Da: (a) AR = 2, B = 2, $Da = 10^{-2}$, (b) AR = 2, B = 6, $Da = 10^{-2}$, (c) AR = 3, B = 6, $Da = 10^{-2}$, and (d) AR = 2, B = 6, $Da = 10^{-1}$.

of the particle, and a third streamline region near and around the surface of the particle. Moreover, we found that for elliptical porous particles with small permeability ($10^{-6} \le Da \le 10^{-3}$), there exist two small vortices to the left and right of the horizontal particle when Re approaches to the Re_c , independent of B. This may be attributed to the pressure distribution near the particle surface.

Finally, our results show that the net torque exerted on the fixed elliptical porous particle at various orientation angles γ and Re in a simple shear flow can be used to estimate whether the corresponding porous particle stops rotating or not. In addition, if the porous particle stops, the variation of net torque can further help to determine χ and Re at which the particle ceases to rotate. When $Re < Re_{cr}$, the net torque at various orientation angles ranging from 0 to π is always positive; hence, the elliptical porous particle rotates with the shear flow and will not stop rotating. When $Re = Re_{cr}$, the curve of net torque vs orientation angles is just tangent to the χ axis, indicating that there is one fixed point where the net torque is 0. The porous particle will stop at this orientation angle and Re. Whereas when $Re > Re_{cr}$, there are two fixed points on the curve of net torque, and only the left fixed point at smaller orientation angle is stable. The elliptical porous particle converges to this stable point ultimately. The linear stability analysis, as shown by the literature, 21-23,38 might provide an alternative way to explain the transition from rotating to stationary state for the porous particles in this work. This, however, will not be discussed in this work and deserve a further publication in the near future.

ACKNOWLEDGMENTS

This work was subsidized by the National Natural Science Foundation of China (Grant No. 91834302).

APPENDIX A: THE NUMERICAL METHOD

The LBM has been shown effective and popular in simulating various complex flow problems because of its accuracy, easy implementation, and natural parallelism.^{39–41} In this work, LBM is employed to solve the macroscopic governing equations (1) and (2). The corresponding LBM equations can be given as

$$f(\mathbf{x} + \mathbf{e}_{\alpha}\delta_{t}, t + \delta_{t}) - f_{\alpha}(\mathbf{x}, t) = -\frac{1}{\tau} \left[f_{\alpha}(\mathbf{x}, t) - f_{\alpha}^{eq}(\mathbf{x}, t) \right] + \delta_{t}F_{\alpha}(\mathbf{x}, t),$$
(A1)

where δ_t is the time step, τ is the relaxation time, F_{α} is the forcing term, and $f_{\alpha}(\mathbf{x},t)$ and $f_{\alpha}^{eq}(\mathbf{x},t)$ are the discrete particle distribution function (PDF) and the equilibrium PDF at position \mathbf{x} and time t,

respectively. For the two-dimensional fluid flows, the discrete velocity set e_{α} in the α direction can be given by

$$\boldsymbol{e}_{\alpha} = \begin{cases} (0,0), & \alpha = 0, \\ c \left(\cos \left[(\alpha - 1) \frac{\pi}{2} \right], \sin \left[(\alpha - 1) \frac{\pi}{2} \right] \right), & \alpha = 1, 2, 3, 4, \\ \sqrt{2}c \left(\cos \left[(2\alpha - 1) \frac{\pi}{4} \right], \sin \left[(2\alpha - 1) \frac{\pi}{4} \right] \right), & \alpha = 5, 6, 7, 8, \end{cases}$$
(A2)

where c is the lattice speed defined as $c = \delta_x/\delta_t$ and δ_x is the lattice size. The forcing term F_α and equilibrium PDF f_α^{eq} in the α direction are, respectively, given by

$$F_{\alpha} = \rho_f \omega_{\alpha} \left(1 - \frac{1}{2\tau} \right) \left[\frac{\boldsymbol{e}_{\alpha}.\boldsymbol{F}_m}{c_s^2} + \frac{\boldsymbol{e}_{\alpha}.\boldsymbol{u}}{c_s^4} (\boldsymbol{e}_{\alpha}.\boldsymbol{F}_m) - \frac{\boldsymbol{u}.\boldsymbol{F}_m}{c_s^2} \right], \quad (A3)$$

$$f_{\alpha}^{eq}(\mathbf{x},t) = \rho_f \omega_{\alpha} \left[1 + \frac{\mathbf{e}_{\alpha} \cdot \mathbf{u}}{c_s^2} + \frac{(\mathbf{e}_{\alpha} \cdot \mathbf{u})^2}{2c_s^4} - \frac{\mathbf{u}^2}{2c_s^2} \right], \tag{A4}$$

where ω_{α} is the weight coefficient defined as $\omega_0 = 4/9$, $\omega_{1-4} = 1/9$, $\omega_{5-8} = 1/36$, c_s is lattice sound speed, and u denotes the intrinsic phase averaged velocity of fluid phase $\langle u_f \rangle^f$. The macroscopic properties related to the PDF can be calculated using

$$\rho_f = \sum_{\alpha=0}^{8} f_{\alpha}, \quad \rho_f \mathbf{u} = \sum_{\alpha=0}^{8} \mathbf{e}_{\alpha} f_{\alpha} + \frac{1}{2} \delta_t \rho_f \mathbf{F}_m. \tag{A5}$$

The macroscopic velocity equation in (A5) is nonlinear because there is \boldsymbol{u} in the total body force \boldsymbol{F}_m as well. By introducing Eq. (4) into Eq. (A5), the quadratic equation can be solved and \boldsymbol{u} is further calculated using

$$u = \frac{v}{d_0 + \sqrt{d_0^2 + d_1 |v|}} + V_p, \tag{A6}$$

and

$$\rho_f \mathbf{v} = \sum_{\alpha=0}^{8} \mathbf{e}_{\alpha} f_{\alpha} + \frac{1}{2} \delta_t \rho_f \mathbf{G} - \rho_f \mathbf{V}_p, \tag{A7}$$

where the two parameters d_0 and d_1 are $d_0 = \frac{1}{2} \left(1 + \frac{1}{2} \delta_t \frac{\varepsilon \nu}{K} \right)$ and $d_1 = \frac{1}{2} \delta_t \frac{\varepsilon^2 F_\varepsilon}{\sqrt{\nu}}$.

In this work, the periodic boundary conditions are imposed in the flow direction, and the non-equilibrium bounce-back schemes are applied to the top and bottom moving bounding walls. Note that no explicit boundary condition is required for the interface between free fluid and the porous particle region, since the viscous term $\mu \nabla^2 \langle \mathbf{u}_f \rangle^f$ has already been included in the macroscopic governing equations to account for the boundary layer occurring in the porous particle flow. For the interactions between fluid and the porous particle, the momentum-exchange method is used to calculate the drag force and torque acting on the particle due to its accuracy and easy implementation. In the momentum-exchange method, it is assumed that the drag force acting on the particle is due to the momentum exchange between the external nodes $\mathbf{x}_f = \mathbf{x}_b + \mathbf{e}_{\overline{a}} \delta t$ and internal boundary nodes within the particle

 x_b , with $e_{\overline{\alpha}}$ being the discrete velocity in the opposite direction of e_{α} (i.e., $e_{\overline{\alpha}} = -e_{\alpha}$). The momentum $e_{\alpha}f_{\alpha}$ which goes into the particle contributes a momentum increment, whereas $e_{\overline{\alpha}}f_{\overline{\alpha}}$ which goes out of the particle contributes a momentum decrement. Therefore, the drag force F_p can be given by

$$F_{p} = \sum_{all \, x_{b}} \sum_{\alpha \neq 0} e_{\alpha} \left[f_{\alpha}(\mathbf{x}_{b}, t) + f_{\overline{\alpha}}(\mathbf{x}_{b} + e_{\overline{\alpha}} \delta_{t}, t) \right] \times \left[1 - w(\mathbf{x}_{b} + e_{\overline{\alpha}} \delta_{t}) \right]. \tag{A8}$$

The torque T_p by

$$T_{p} = \sum_{\text{all } x_{b}} \sum_{\alpha \neq 0} (\mathbf{x}_{b} - \mathbf{R}) \times [\mathbf{e}_{\alpha} [f_{\alpha}(\mathbf{x}_{b}, t) + f_{\overline{\alpha}}(\mathbf{x}_{b} + \mathbf{e}_{\overline{\alpha}} \delta_{t}, t)] \times [1 - w(\mathbf{x}_{b} + \mathbf{e}_{\overline{\alpha}} \delta_{t})]]. \tag{A9}$$

Here, w(i,j) is a scalar array where a value of 1 is assigned for those lattice sites (i,j) within the particle and a value of 0 is assigned for those fluid lattice nodes occupied by fluid.

APPENDIX B: THE ROTATION PERIOD FOR H/D=3 AND 5

Figures 15 and 16 show the dimensionless rotation period ΓT as a function of Re for elliptical porous particles (AR=2) for B=3 and B=5, respectively. The two fitting parameters C and Re_c are listed in Table VI. By comparing Tables VI and II, we find that Re_c for H/D=3 is larger than that for H/D=4 and smaller than that for H/D=2 for a fixed Da. For example, for $Da=2\times 10^{-2}$, $Re_c=61.73$ for H/D=3, whereas $Re_c=72.00$ and $Re_c=57.62$ for H/D=2 and H/D=4, respectively. This means that the confinement effects at H/D=3 cannot be neglected. For H/D=5, the comparison between the results in Tables VI and II supports that the confinement effects can be neglected.

Figures 17 and 18 show the dimensionless rotation period ΓT as a function of Re for elliptical porous particles with AR = 2.5

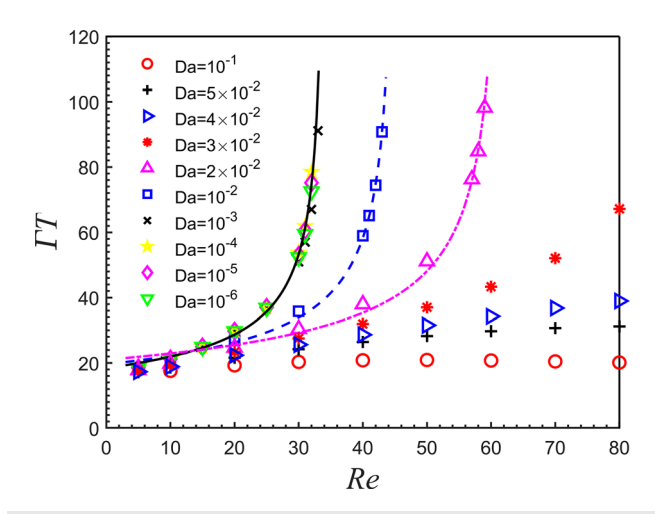


FIG. 15. The dimensionless rotation period ΓT as a function of Re for elliptical porous particles with AR=2 and H/D=3 where Da is ranging from 10^{-6} to 10^{-1} .

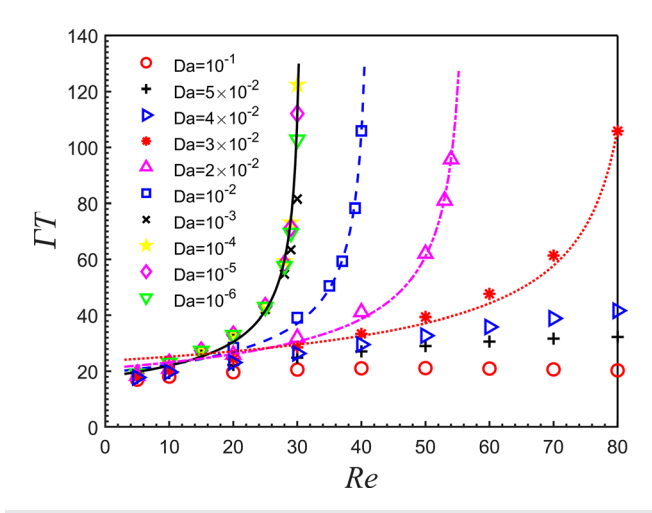


FIG. 16. The dimensionless rotation period ΓT as a function of Re for elliptical porous particles with AR=2 and H/D=5 where Da is ranging from 10^{-6} to 10^{-1} .

TABLE VI. The fitting parameters C and Re_c in the scaling law $\Gamma T = C(Re_c - Re)^{-1/2}$ for the elliptical porous particles with AR = 2, B = 3, 5, and $10^{-6} \le Da \le 2 \times 10^{-2}$.

AR	B = H/D	Da	С	Re_c
2	3	$ 2 \times 10^{-2} \\ 10^{-2} \\ 10^{-3} \sim 10^{-6} $	164.92 131.72 107.70	61.73 45.10 34.08
2	5	$ \begin{array}{c} 10 & \sim 10 \\ 2 \times 10^{-2} \\ 10^{-2} \\ 10^{-3} \sim 10^{-6} \end{array} $	158.51 125.44 100.43	56.75 41.43 30.82

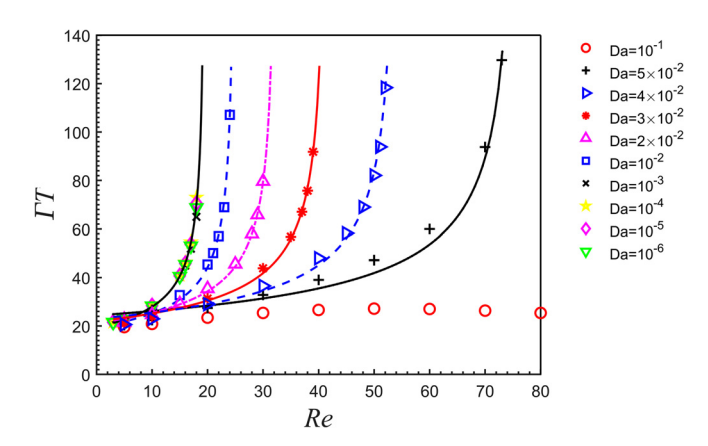


FIG. 17. The dimensionless rotation period ΓT as a function of Re for elliptical porous particles with AR=2.5 and H/D=3 where Da is ranging from 10^{-6} to 10^{-1} .

under B = 3 and 5, respectively. The two fitting parameters C and Re_c are listed in Table VII. Comparison between Tables VII and III shows that the confinement effects cannot be neglected for H/D = 3.

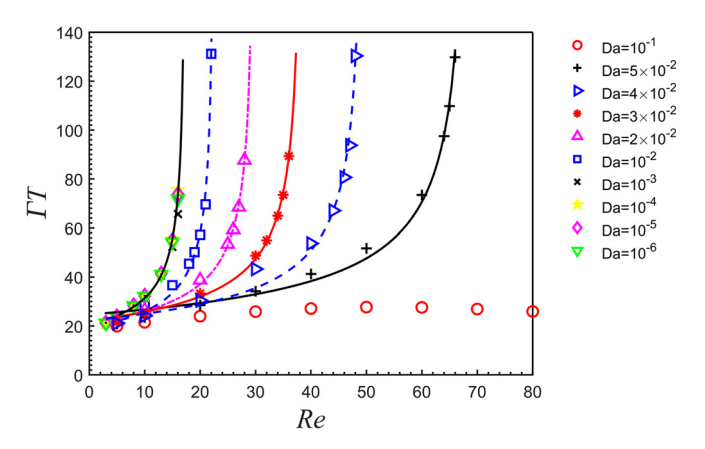


FIG. 18. The dimensionless rotation period ΓT as a function of Re for elliptical porous particles with AR=2.5 and H/D=5 where Da is ranging from 10^{-6} to 10^{-1} .

TABLE VII. The fitting parameters C and Re_c in the scaling law $\Gamma T=C(Re_c-Re)^{-1/2}$ for the elliptical porous particles with AR=2.5, B=3, 5, and $10^{-6} \leq Da \leq 5 \times 10^{-2}.$

\overline{AR}	B = H/D	Da	С	Re_c
2.5	3	5×10^{-2}	212.05	75.63
		$4 imes 10^{-2}$	169.43	54.10
		$3 imes 10^{-2}$	141.08	41.38
		2×10^{-2}	120.42	32.30
		10^{-2}	97.23	24.84
		$10^{-3}\sim 10^{-6}$	86.21	19.51
2.5	5	$5 imes 10^{-2}$	204.24	68.37
		$4 imes 10^{-2}$	157.10	49.52
		$3 imes 10^{-2}$	137.32	38.39
		2×10^{-2}	116.06	29.77
		10^{-2}	91.81	22.50
		$10^{-3} \sim 10^{-6}$	84.95	17.33

DATA AVAILABILITY

The data that support the findings of this study are available from the corresponding author upon reasonable request.

REFERENCES

¹B. Kärcher, "Homogeneous ice formation in convective cloud outflow regions," Q. J. R. Meteorol. Soc. **143**, 2093 (2017).

²J. S. Guasto, R. Rusconi, and R. Stocker, "Fluid mechanics of Planktonic micro-organisms," Annu. Rev. Fluid Mech. 44, 373 (2012).

³H. S. Auta, C. U. Emenike, and S. H. Fauziah, "Distribution and importance of microplastics in the marine environment: A review of the sources, fate, effects, and potential solutions," Environ. Int. 102, 165 (2017).

⁴S. Blaser, "Flocs in shear and strain flows," J. Colloid Interface Sci. 225, 273 (2000).

⁵P. Tian, Y. Wei, M. Ye, and Z. Liu, "Methanol to olefins (MTO): From fundamentals to commercialization," ACS Catal. 5, 1922 (2015).

⁶F. Lundell, L. D. Söderberg, and P. H. Alfredsson, "Fluid mechanics of paper-making," Annu. Rev. Fluid Mech. 43, 195 (2011).

- ⁷G. B. Jeffery, "The motion of ellipsoidal particles immersed in a viscous fluid," Proc. R. Soc. London, Ser. A 102, 161 (1922).
- ⁸C. R. Robertson and A. Acrivos, "Low Reynolds number shear flow past a rotating circular cylinder. Part 1. Momentum transfer," J. Fluid Mech. **40**, 685 (1970).
- ⁹J. Einarsson, F. Candelier, F. Lundell, J. R. Angilella, and B. Mehlig, "Rotation of a spheroid in a simple shear at small Reynolds number," Phys. Fluids 27, 063301 (2015).
- 10 E. Y. Harper and I.-D. Chang, "Maximum dissipation resulting from lift in a slow viscous shear flow," J. Fluid Mech. 33, 209 (1968).
- ¹¹L. G. Leal, "The slow motion of slender rod-like particles in a second-order fluid," J. Fluid Mech. 69, 305 (1975).
- ¹²C. A. Kossack and A. Acrivos, "Steady simple shear flow past a circular cylinder at moderate Reynolds numbers: A numerical solution," J. Fluid Mech. 66, 353 (1974).
- ¹³E.-J. Ding and C. K. Aidun, "The dynamics and scaling law for particles suspended in shear flow with inertia," J. Fluid Mech. 423, 317 (2000).
- ¹⁴T. Rezaee and K. Sadeghy, "Effect of porosity on the settling behavior of a 2D elliptic particle in a narrow vessel: A lattice-Boltzmann simulation," Phys. Fluids 31, 123301 (2019).
- ¹⁵S.-L. Huang, S.-D. Chen, T.-W. Pan, C.-C. Chang, and C.-C. Chu, "The motion of a neutrally buoyant particle of an elliptic shape in two dimensional shear flow: A numerical study," Phys. Fluids 27, 083303 (2015).
- ¹⁶G. G. Poe and A. Acrivos, "Closed-streamline flows past rotating single cylinders and spheres: Inertia effects," J. Fluid Mech. 72, 605 (1975).
- ¹⁷C. M. Zettner and M. Yoda, "The circular cylinder in simple shear at moderate Reynolds numbers: An experimental study," Exp. Fluids 30, 346 (2001).
- ¹⁸C. M. Zettner and M. Yoda, "Moderate-aspect-ratio elliptical cylinders in simple shear with inertia," J. Fluid Mech. 442, 241 (2001).
- ¹⁹D. W. Qi and L.-S. Luo, "Rotational and orientational behaviour of three-dimensional spheroidal particles in Couette flows," J. Fluid Mech. 477, 201 (2003).
- ²⁰F. Lundell and A. Carlsson, "Heavy ellipsoids in creeping shear flow: Transitions of the particle rotation rate and orbit shape," Phys. Rev. E 81, 016323 (2010).
- ²¹F. Lundell, "The effect of particle inertia on triaxial ellipsoids in creeping shear: From drift toward chaos to a single periodic solution," Phys. Fluids 23, 011704 (2011).
- ²²T. Rosen, Y. Kotsubo, C. K. Aidun, M. Do-Quang, and F. Lundell, "Orientational dynamics of a triaxial ellipsoid in simple shear flow: Influence of inertia," Phys. Rev. E 96, 013109 (2017).
- 23T. Rosén, A. Nordmark, C. K. Aidun, M. Do-Quang, and F. Lundell, "Quantitative analysis of the angular dynamics of a single spheroid in simple shear flow at moderate Reynolds numbers," Phys. Rev. Fluids 1, 044201 (2016).
- ²⁴Z. Cui, L. Zhao, W. Huang, and C. Xu, "Stability analysis of rotational dynamics of ellipsoids in simple shear flow," Phys. Fluids 31, 023301 (2019).

- ²⁵H. Masoud, H. A. Stone, and M. J. Shelley, "On the rotation of porous ellipsoids in simple shear flows," J. Fluid Mech. 733, R6 (2013).
- 26L. Wang, L.-P. Wang, Z. Guo, and J. Mi, "Volume-averaged macroscopic equation for fluid flow in moving porous media," Int. J. Heat Mass Transfer 82, 357 (2015).
- 27 C. Li, M. Ye, and Z. Liu, "On the rotation of a circular porous particle in 2D simple shear flow with fluid inertia," J. Fluid Mech. 808, R3 (2016).
- ²⁸ A. Xu, L. Shi, and T. S. Zhao, "Lattice Boltzmann simulation of shear viscosity of suspensions containing porous particles," Int. J. Heat Mass Transfer 116, 969 (2018).
- ²⁹X. Liu, H. Huang, and X.-Y. Lu, "Lattice Boltzmann study of effective viscosities of porous particle suspensions," Comput. Fluids 181, 135 (2019).
- ³⁰J. Liu, C. Li, M. Ye, and Z. Liu, "The rotation of two-dimensional elliptical porous particles in a simple shear flow with fluid inertia," Phys. Fluids 32, 043305 (2020).
- ³¹S. Bhattacharyya, S. Dhinakaran, and A. Khalili, "Fluid motion around and through a porous cylinder," Chem. Eng. Sci. 61, 4451 (2006).
- ³²S. Ergun, "Fluid flow through pached columns," Chem. Eng. Prog. 48, 89 (1952).
- 33J. Feng and D. D. Joseph, "The unsteady motion of solid bodies in creeping flows," J. Fluid Mech. 303, 83 (1995).
- 34S. Forrest, "Genetic algorithms: Principles of natural selection applied to computation," Science 261, 872 (1993).
- 35 M. Schmidt and H. Lipson, "Distilling free-form natural laws from experimental data," Science 324, 81 (2009).
- ³⁶H. Vaddireddy, A. Rasheed, A. E. Staples, and O. San, "Feature engineering and symbolic regression methods for detecting hidden physics from sparse sensor observation data," Phys. Fluids 32, 015113 (2020).
- 37W. Cai, A. Pacheco-Vega, M. Sen, and K. T. Yang, "Heat transfer correlations by symbolic regression," Int. J. Heat Mass Transfer 49, 4352 (2006).
- ³⁸ M. Sun, "Insect flight dynamics: Stability and control," Rev. Mod. Phys. 86, 615 (2014).
- 39Z. Guo and T. S. Zhao, "Lattice Boltzmann model for incompressible flows through porous media," Phys. Rev. E 66, 036304 (2002).
- ⁴⁰M. A. V. D. Hoef, R. Beetstra, and J. A. M. Kuipers, "Lattice-Boltzmann simulations of low-Reynolds-number flow past mono- and bidisperse arrays of spheres: Results for the permeability and drag force," J. Fluid Mech. **528**, 233 (2005)
- ⁴¹H. Li, F. Y. Leong, G. Xu, Z. Ge, C. W. Kang, and K. H. Lim, "Motion of a neutrally buoyant circular particle in a clockwise double-lid-driven square cavity," Phys. Fluids 32, 113301 (2020).
- ⁴²Q. Zou and X. He, "On pressure and velocity boundary conditions for the lattice Boltzmann BGK model," Phys. Fluids 9, 1591 (1997).
- ⁴³R. Mei, D. Yu, W. Shyy, and L. S. Luo, "Force evaluation in the lattice Boltzmann method involving curved geometry," Phys. Rev. E 65, 041203 (2002).